

Female mice lacking p47^{phox} have altered adipose tissue gene expression and are protected against high fat-induced obesity

Martin J. J. Ronis, Neha Sharma, Jamie Vantrease, Sarah J. Borengasser, Matthew Ferguson, Kelly E. Mercer, Mario A. Cleves, Horacio Gomez-Acevedo and Thomas M. Badger

Physiol. Genomics 45:351-366, 2013. First published 12 March 2013;
doi: 10.1152/physiolgenomics.00148.2012

You might find this additional info useful...

Supplementary material for this article can be found at:

<http://physiolgenomics.physiology.org/http://physiolgenomics.physiology.org/content/suppl/2013/03/20/physiolgenomics.00148.2012.DC1.html>

This article cites 45 articles, 18 of which you can access for free at:

<http://physiolgenomics.physiology.org/content/45/9/351.full#ref-list-1>

Updated information and services including high resolution figures, can be found at:

<http://physiolgenomics.physiology.org/content/45/9/351.full>

Additional material and information about *Physiological Genomics* can be found at:

<http://www.the-aps.org/publications/physiolgenomics>

This information is current as of May 2, 2013.

Physiological Genomics publishes results of a wide variety of studies from human and from informative model systems with techniques linking genes and pathways to physiology, from prokaryotes to eukaryotes. It is published 24 times a year (twice monthly) by the American Physiological Society, 9650 Rockville Pike, Bethesda MD 20814-3991. Copyright © 2013 the American Physiological Society. ISSN: 1531-2267. Visit our website at <http://www.the-aps.org/>.

Female mice lacking p47^{phox} have altered adipose tissue gene expression and are protected against high fat-induced obesity

Martin J. J. Ronis,^{1,2,3} Neha Sharma,¹ Jamie Vantrease,¹ Sarah J. Borengasser,^{1,3} Matthew Ferguson,¹ Kelly E. Mercer,² Mario A. Cleves,^{1,2} Horacio Gomez-Acevedo,^{1,3} and Thomas M. Badger^{1,2,4}

¹Arkansas Children's Nutrition Center, University of Arkansas for Medical Sciences, Little Rock, Arkansas; ²Department of Pediatrics, University of Arkansas for Medical Sciences, Little Rock, Arkansas; ³Department of Pharmacology & Toxicology, University of Arkansas for Medical Sciences, Little Rock, Arkansas; and ⁴Department of Physiology & Biophysics, University of Arkansas for Medical Sciences, Little Rock, Arkansas

Submitted 7 November 2012; accepted in final form 7 March 2013

Ronis MJ, Sharma N, Vantrease J, Borengasser SJ, Ferguson M, Mercer KE, Cleves MA, Gomez-Acevedo H, Badger TM. Female mice lacking p47^{phox} have altered adipose tissue gene expression and are protected against high fat-induced obesity. *Physiol Genomics* 45: 351–366, 2013. First published March 12, 2013; doi:10.1152/physiolgenomics.00148.2012.—The current study was designed to determine if the NADPH-oxidase NOX2 plays a role in development of obesity after high fat feeding. Wild-type (WT) mice and mice lacking the essential cytosolic NOX2 system component p47^{phox} (P47KO mice) were fed AIN-93G diets or high-fat diets (HFD) containing 45% fat and 0.5% cholesterol for 13 wk from weaning. Fat mass was increased to a similar degree by HFD in males of both genotypes ($P < 0.05$). However, female P47KO-HFD mice had no increase in adiposity or adipocyte size relative to female WT-HFD mice. Resistance to HFD-driven obesity in P47KO females was associated with increased expression of hepatic TFAM and UCP-2 mRNA, markers of mitochondrial number and uncoupling, and increased expression of hepatic mitochondrial respiratory complexes and whole body energy expenditure in response to HFD. Microarray analysis revealed significantly lower expression of mRNA encoding genes linked to energy metabolism, adipocyte differentiation (PPAR γ), and fatty acid uptake (CD36, lipoprotein lipase), in fat pads from female P47KO-HFD mice compared with WT-HFD females. Moreover, differentiation of preadipocytes *ex vivo* was suppressed more by 17 β -estradiol in cells from P47KO compared with cells from WT females in conjunction with overexpression of mRNA for Pref-1 ($P < 0.05$). HFD mice of both sexes were resistant to the development of hyperglycemia and hepatic steatosis ($P < 0.05$) and had reduced serum triglycerides, leptin, and adiponectin relative to WT-HFD mice ($P < 0.05$). These data suggest that NOX2 is an important regulator of metabolic homeostasis and diet-induced obesity.

adipose; metabolism; NADPH-oxidase; obesity; p47^{phox}

THE FAMILY OF NADPH oxidase (NOX) enzymes is a major source of reactive oxygen species (ROS) utilized in many cell types for redox-based signaling pathways (19). Seven mammalian Nox enzymes (NOX1–NOX5, Duox1, and Duox2) have been described (19). Of these, NOX1–NOX3 consist of a membrane embedded heterodimer (a flavocytochrome oxidase and p22^{phox}) and a number of cytoplasmic regulators that are recruited to the membrane on enzyme activation and that are essential for NADPH oxidase activity and ROS generation (19). In the case of the best-described NOX enzyme, NOX2, these regulators include the small GTPase Rac, bound to GTP,

and the GTP-dependent target proteins: NOX activator p67^{phox} and the adaptor protein p47^{phox} (19). NOX2 was originally characterized as the mediator of host-defense action in phagocytic cells such as macrophages and Kupffer cells present in adipose tissue and in the liver (6, 11, 19). However, NOX2 has more recently been reported to be present in a wide variety of other adipose tissue cell types including preadipocytes, differentiated mature adipocytes, and endothelial cells (23, 28, 36). Another NOX enzyme, NOX4, which is constitutively active and does not require complex formation with cytosolic regulators for ROS formation (19), has also been found in adipose tissue, predominantly in mesenchymal stem cells and preadipocytes (13, 17, 36).

It is well known that there is low-level inflammation associated with the development of obesity (18). However, the relationship between inflammation, oxidative stress, NOX-dependent ROS and redox signaling in adipose tissue, and regulation of adipocyte differentiation and hyperplasia in response to high-fat feeding is not well understood (7). Expression of NOX2, p22^{phox}, p40^{phox}, p47^{phox}, and NOX4 has been shown to be increased in adipose tissue and vasculature of genetically obese mice and mice with diet-induced obesity (7, 23, 25, 39). In addition, NOX4 has been shown to be elevated in adipose tissue from humans with extreme insulin resistance and in obese Pima Indians compared with lean subjects (18, 26). *In vitro* studies with mesenchymal stem cell lines and preadipocytes suggest that NOX4-dependent ROS signaling is a switch responsible for inhibiting insulin-induced preadipocyte proliferation while stimulating adipocyte differentiation. In addition, NOX4 expression was shown to be reduced during adipocyte differentiation (13, 17, 36). However, more recent *in vivo* studies in NOX4-deficient male mice have demonstrated increased whole body energy efficiency and predisposition toward diet-induced obesity, insulin resistance, adipose tissue inflammation, and hepatic steatosis (21). These data suggest NOX4 is actually an antiadipogenic master regulator of metabolic homeostasis and that its upregulation in obese adipose tissue might represent a defensive mechanism to limit adipose tissue expansion (21). In contrast, less is known with regard to the role of NOX2 in adipogenesis and obesity. One report suggested that male mice with inactive NOX2 as a result of p47^{phox} deficiency are protected against high fat-induced adipose tissue inflammation and systemic insulin resistance (43). Another recent study linked induction of p47^{phox} mRNA expression in differentiated adipocytes *in vitro* by the obesity-associated ETS transcription factor PU.1 with ROS generation, activation of the MAP kinase JNK, and inhibition

Address for reprint requests and other correspondence: M. J. J. Ronis, Arkansas Children's Nutrition Center, 15 Children's Way, Little Rock, AR 72202 (e-mail: RonisMartinJ@uams.edu).

of insulin signaling and cytokine production (23). p47^{phox} expression in hepatic parenchymal cells has also been linked to development of alcoholic steatosis (20).

Here we investigated the adipogenic response and metabolic phenotype of male and female mice with genetic ablation of the *Ncf1* gene, which encodes p47^{phox} (P47KO mice) fed either a control semipurified AIN-93G diet or a typical high-fat “Western” diet (HFD) containing 45% fat and 0.5% cholesterol during early development. Our data demonstrate that in the absence of p47^{phox}, male mice were resistant to high fat feeding-induced hyperglycemia and hepatic steatosis. However, P47KO female mice were also leaner than wild-type mice; were resistant to high fat-induced obesity; had increased energy expenditure associated with increased mitochondrial respiration, altered adipocyte differentiation and lipogenesis; and had suppressed adipokine production.

MATERIALS AND METHODS

Mice and diets. The experiments received prior approval from the Institutional Animal Care and Use Committee at the University of Arkansas for Medical Sciences. Time-impregnated female wild-type C57BL/6 (WT) and C57BL/6J-*Ncf1*^{M1J/J} (P47KO) mice were obtained from Jackson Labs (Bar Harbor, ME). Dams and litters were housed in polycarbonate cages in an Association of Laboratory Animal Care-approved animal facility in an environmentally controlled room at 22°C with a 12 h light/dark cycle and fed standard rodent chow ad libitum throughout pregnancy and lactation. At weaning (postnatal day 28), male and female WT and P47KO pups ($n = 10$ /group) were fed ad libitum with a semipurified control AIN-93G diet formulated with casein as the sole protein source as previously described (32), for 13 wk (AIN-93G). Additional groups of WT and P47KO male and female pups ($n = 10$) were fed a high-fat “Western” diet (Harlan Teklad TD88137) containing 42% fat energy, mainly from milk fat + 0.5% cholesterol also made with casein as the sole protein source for 13 wk (HFD). Body weights were recorded on a weekly basis. Food intake was recorded daily for 7 days after 1, 4, and 12 wk on diet. After 11 wk on diet, blood glucose and insulin values were determined in submandibular blood drawn after an overnight fast. Also after 11 wk on diet, P47KO mice were placed in metabolic chambers for 48 h using the Complete Lab Animal Monitoring System (CLAMS) to assess energy expenditure (EE) and respiratory exchange ratio (RER) (Columbus Instruments, Columbus, OH). EE and RER data from the final 24 h was utilized for conversion into percent relative cumulative frequency (PRCF) values as described previously (2). After the mice were killed, serum, liver, and retroperitoneal fat pads were collected and stored at -70°C until use.

Body composition analysis. Body composition was assessed via whole animal NMR (Echo Medical Systems, Houston, TX) performed in conscious unanesthetized mice (37) and by postmortem dissected

weights of retroperitoneal abdominal fat pads. Adipose tissue histomorphometric analysis was carried out as described previously (37). Retroperitoneal fat deposits (in 3–4 mm pieces) were fixed in buffered alcoholic formalin for 4 days and embedded in paraffin. Sections (6 μ m) were stained with hematoxylin and eosin. Diameters of adipocytes were measured under a Zeiss Axiovert microscope (Carl Zeiss, Thornwood, NY) with Zeiss Vision software. A minimum of 300 cells at random were measured for each slide, and the percentage cells in each size range was computed with MS Excel (Microsoft, Redmond, WA).

Biochemical analysis. Serum nonesterified free fatty acids (NEFA) were measured using the NEFA C kit from Waco Chemicals (Richmond, VA). Serum triglycerides were measured using triglyceride reagent (IR141; Synermed, Westfield, IN). Triglyceride was extracted from whole liver homogenates with chloroform-methanol (2:1, vol/vol) and analyzed using triglyceride reagent (IR141, Synermed). Serum glucose concentrations were measured using glucose reagent (IR071-072, Synermed). Serum insulin and leptin concentrations were measured using ELISA kits from Linco Research (St. Charles, MO) according to manufacturer’s protocols. Serum adiponectin concentrations were measured using an ELISA kit from B-Bridge International (Sunnyvale, CA) according to manufacturer’s protocols. Liver mitochondrial protein extracts were prepared using a Mitochondrial Isolation kit for Tissue (Pierce, Rockford, IL), and immunoblotting was performed for oxidative phosphorylation complexes I–V (MitoSciences, Eugene, OR). Mitochondrial numbers were estimated indirectly by real-time RT-PCR analysis of expression of the mitochondrial transcription factor mtTFAM mRNA. Expression of the uncoupling protein UCP-2 mRNA was analyzed by real-time RT-PCR (2).

Adipose tissue gene expression analysis. Gene expression profiles from the retroperitoneal abdominal fat pads of female WT and P47KO mice were assessed using GeneChip Mouse Genome 430 2.0 microarrays (Affymetrix, Santa Clara, CA) containing 45,000 probe sets, with ~39,000 transcripts and variants. Total RNA was extracted, and three pools were prepared from each treatment group, each pool generated from $n = 3$ –4 different fat pads. The intensity values of different probe sets (genes) generated by Affymetrix GeneChip Software were imported into GeneSpring version 11.5 software (Agilent Technologies, Santa Clara, CA) for data analysis. The data files (CEL files) containing the probe level intensities were processed using the robust multiarray average algorithm, for background correction, log₂-transformation, and quantile normalization of the perfect match probe level values (30, 31). For comparison analysis, genes were filtered based on minimum 1.5-fold ratio change and P value ≤ 0.05 using Student’s t -test followed by Benjamini and Hochberg false discovery rate. Features were classified using hierarchical clustering with Euclidean distance. Visualization of data was accomplished using GeneSpring GX v11.0.2. Known biological functions of genes were queried and acquired from Affymetrix online data analysis resource NetAffx and gene ontology (GO) analyses performed using Affymetrix GO

Table 1. Real-time primer sequences used in the current study

Gene	NCBI Reference Sequence	Amplicon Length	Forward Sequence (5'-3')	Reverse Sequence (5'-3')
<i>m-LPL</i>	NM_008509.2	174	ACGAGCGTCCATTCATCTCTTCA	TGCTTCTCTTGCTCTGACCTTGT
<i>m-TFAM</i>	NM_009360.4	113	TTCTTGGGAAGAGCAGATGGCTGAA	TCCCAATGACAACTCCGTCTTCCA
<i>m-CD36</i>	NM_001159555.1	101	CTGTGTCTTTGTACAGGCCAATG	AGCTGCTACAGCCAGATTCAGAA
<i>m-PPARγ</i>	NM_001127330.1	101	GCTTCCACTATGGAGTTCATGCT	CCGGCAGTTAAGATCACACCTAT
<i>m-FASn</i>	NM_007988.3	116	TGACCTCGTGTAGCAACGTGATC	GGGTGAGGACGTTTACAAGG
<i>m-UCP-2</i>	NM_011671.4	101	AAGACCATTGCACGAGAGGAA	TAGGTACCAGCTCAGTACAGTTGA
<i>m-UCP-1</i>	NM_009463.3	193	AACACCTGCCTCTCTCGGAAACAA	TGTTGACAAGCTTCTGTGGTGGC
<i>m-Runx-2</i>	NM_001145920.1	108	CGGTCTCCTTCCAGGATGGT	GCTTCCGTCCAGGCTCAACA
<i>m-PGC-1α</i>	NM_008904.2	101	GTGTTCCCGATCACCATATTCC	GGTGTCTGTAGTGGCTTGATTTCAT
<i>m-PREF-1</i>	NM_001190705.1	133	GCTACAACCACATGCTTCGCAAGA	ATCCTCATCCAGCCCTCCTTGT

NCBI, National Center for Biotechnology Information; m, *Mus musculus*.

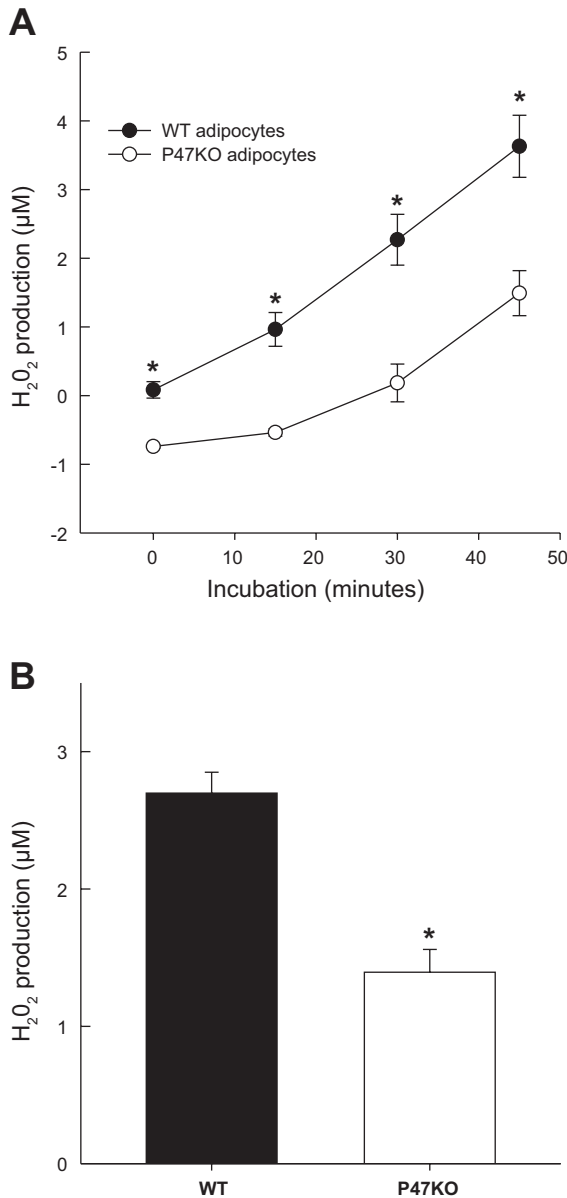


Fig. 1. Basal (A) and PMA-stimulated (B) hydrogen peroxide (H₂O₂) generation was measured in wild-type (WT) and p47^{phox} ^{-/-} (P47KO) ex vivo stromal vascular (SV) cultures using the Amplex Red hydrogen peroxide/ peroxidase assay kit as described in MATERIALS AND METHODS. Data are expressed as the amount produced (μM) at each time point. Statistical significance was determined by Student's *t*-test for every time point, **P* < 0.05.

Browser (31). Analysis of genes mapped to biological pathways was conducted using Affymetrix NetAffx and GO analysis for biological/ molecular function performed using GeneSpring using false discovery rate of *P* < 0.1 (default for Gene Spring) (31). Furthermore, the lists of genes with significantly different expression in fat pads from WT AIN-93G vs. P47KO AIN-93G mice, WT AIN-93G vs. WT HFD, P47KO AIN-93G vs. P47KO HFD, and WT HFD vs. P47KO HFD were analyzed using DAVID to perform functional annotation. This analysis included identifying top interacting networks based on gene databases from the known literature as described previously for other mRNA data sets (31). Confirmation of microarray gene expression data was done by real-time RT-PCR.

Real-time RT-PCR. Total RNA was extracted from livers and retroperitoneal abdominal fat using TRI reagent and cleaned using

RNeasy mini columns (Qiagen, Valencia, CA). RNA quality was ascertained spectrophotometrically (ratio of A260/A280) and also by checking ratio of 28S to 18S ribosomal RNA using the RNA Nano Chip on a 2100 Bioanalyzer (Agilent Technologies, Palo Alto, CA). Total RNA (1 μg) was reverse transcribed using the iScript Reverse Transcription kit (Bio-Rad Laboratories, Hercules, CA) according to manufacturer's instructions. The reverse transcribed cDNA (10 ng) was utilized for real-time PCR (RT-PCR) using the 2X SYBR green master mix and monitored on a ABI Prism 7000 sequence detection system (Applied Biosystems, Foster City, CA). Gene-specific oligonucleotide probes were designed using Primer Express Software (Applied Biosystems) (Table 1), and the relative amounts of gene expression were quantitated using a standard curve according to manufacturer's instructions and normalized against expression of 18S rRNA.

Western blot analysis of protein expression. Western blots of whole tissue homogenates were utilized to confirm effects of P47^{phox} genotype and HFD feeding on mRNAs at the level of protein expression. PPARγ and CD36 protein expression was determined in female mouse adipose tissue using gonadal fat pads and methods previously described (31, 38). Expression of lipoprotein lipase (LPL) protein was analyzed in gonadal fat pads using a monoclonal antibody from Abcam (ab21356). Expression of target proteins was normalized against total protein loaded based on Amido black staining of whole lanes.

Isolation of stromal vascular cells and ex vivo differentiation. Stromal vascular (SV) cells were isolated from adipose tissue taken from chow-fed WT and P47KO female and male mice at age 6 wk (*n* = 5/group) using collagenase digestion as previously described (40). SV cells were plated in 12-well plates (3 × 10⁵ cells/well) and cultured for 7 days with or without estradiol (1 nM), and adipogenic differentiation was induced in 2 days postconfluent cells by supplementation of MDI (0.5 mM methyl-isobutyl-xanthine, 0.5 μM dexamethasone, and 10 μg/ml insulin) in differentiation medium (DMEM + 10% FBS). The MDI supplemented medium was replaced with medium containing insulin (10 μg/ml) alone on day 2, followed by medium without supplementation from day 4 to 8. On day 8, cells

Table 2. Effect of p47^{phox} genotype and diet on mouse body and fat pad weights

Group	Food Intake, kcal/day/kg	Weight, g	% Weight Gain	Fat, %
<i>Male</i>				
WT:AIN-93G	212 ± 12	29.4 ± 0.8 ^{a*}	148 ± 6 ^{a†}	3.8 ± 0.3 ^a
P47KO:AIN-93	212 ± 13	31.6 ± 0.6 ^{a†}	123 ± 5 [*]	3.7 ± 0.4 ^a
WT:HFD	187 ± 12	33.5 ± 1.1 ^b	198 ± 5 ^{b,†}	5.4 ± 0.6 ^b
P47KO:HFD	198 ± 13	34.7 ± 1.1 ^b	141 ± 10 [*]	5.5 ± 0.5 ^b
<i>Female</i>				
WT:AIN-93G	202 ± 12	23.4 ± 0.5 ^a	108 ± 5 ^{a†}	2.8 ± 0.2 ^{a†}
P47KO:AIN-93G	202 ± 8	22.2 ± 0.4	62 ± 1 [*]	1.7 ± 0.1 [*]
WT:HFD	197 ± 7	26.4 ± 1.1 ^{b,†}	146 ± 6 ^{b,†}	3.8 ± 0.5 ^{b,†}
P47KO:HFD	229 ± 12	22.6 ± 0.4 [*]	68 ± 3 [*]	1.6 ± 0.1 [*]

Data are means ± SE (*n* = 10 mice/group). Average food intake during experimental feeding period (kcal/day/kg); Body weight at sacrifice (g); Weight gain as % of initial body weight; wt of abdominal fat pad as % body weight. WT, wild-type mice; P47KO, p47^{phox} ^{-/-} mice; AIN-93G, fed AIN-93G diet; HFD, fed high-fat/high-cholesterol diet as described in MATERIALS AND METHODS. Means bearing different letters differ significantly by diet within genotype *P* < 0.05, a < b, means bearing different symbols are significantly different by genotype within diet, * < †, *P* < 0.05 based on 2-way ANOVA followed by Student-Neuman-Keuls post hoc analysis within each sex.

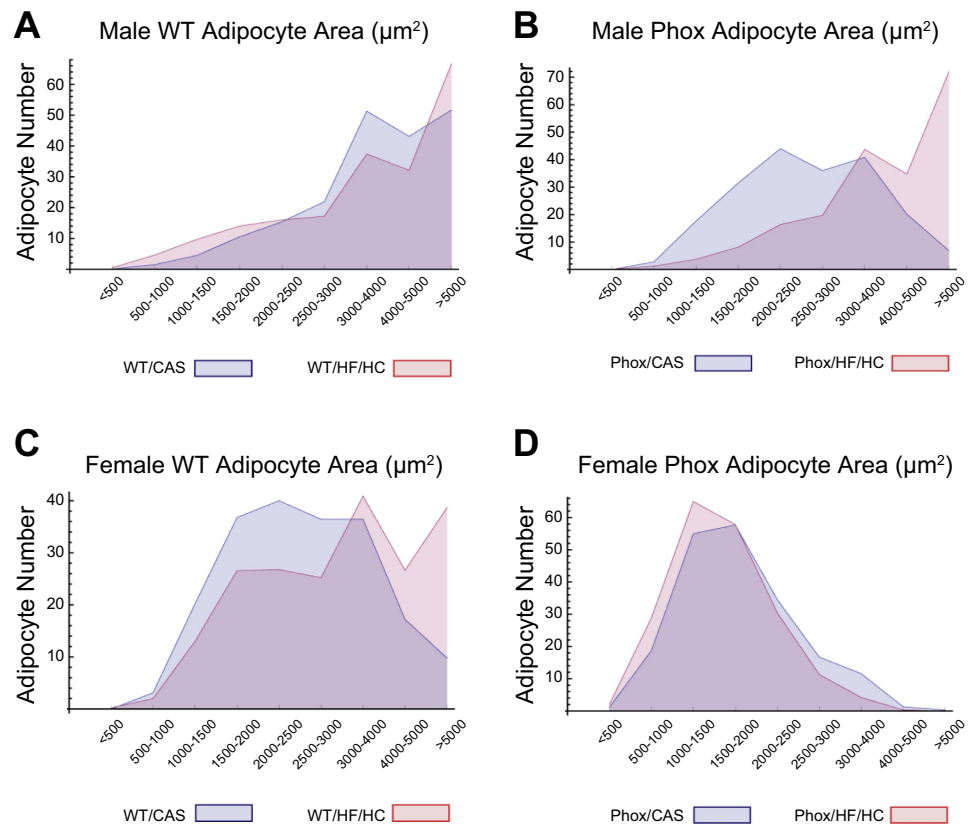


Fig. 2. Analysis of adipocyte size distribution in the abdominal fat pad of WT or P47KO mice fed AIN-93G (AIN-93G) or high-fat diets (HFD).

were stained for lipid droplets using oil red O. Oil red O-positive cells were counted, and total RNA was extracted for RT-PCR analysis of mRNA expression as described above.

ROS production in SV cells isolated from fat pads of WT and P47KO mice. Basal and phorbol 12-myristate-13-acetate (PMA)-stimulated hydrogen peroxide production was measured in SV cells

freshly isolated from the retroperitoneal abdominal fat pads of 6 wk old mice using the Amplex Red hydrogen peroxide/peroxidase assay (Invitrogen Molecular Probes, Eugene, OR) as per manufacturer's instructions. Hydrogen peroxide is derived from the action of the enzyme superoxide dismutase on NOX-generated superoxide, and PMA is a known stimulator of NOX2 activity (27). To measure basal hydrogen peroxide concentrations, the SV cells from chow-fed female WT and P47KO mice were washed twice in Ringer's solution and plated (20,000 cells/well) in triplicate into wells of a 96-well plate containing 50 μl of Amplex Red reaction buffer (50 μM Amplex red, 0.1 U/ml horseradish peroxidase) and incubated at 37°C continuously for 45 min. Absorbance readings at 560 nm were taken at 15 min intervals, and the amount of hydrogen peroxide produced (μM) was plotted against incubation time. SV cells (20,000 cells) were also incubated with Amplex Red reaction buffer with, or without, PMA (12.5 ng/ml) at 37°C for 15 min. Data were expressed as amount of hydrogen peroxide produced (μM), corrected for nonspecific hydrogen peroxide production by subtracting experimental values from values obtained from control wells not containing PMA. Similar results were obtained in a repeat experiment performed in triplicate.

Statistical analysis. Data are presented as means ± SE. Two-way analysis of variance (ANOVA) was used to test overall mean differences based on genotype (WT vs. P47KO), diet (AIN-93G vs. HFD), or genotype × diet interactions with data from each sex analyzed separately. Post hoc comparisons of means were performed by an all-pair-wise Student-Newman-Keuls comparison test and considered significant if $P \leq 0.05$. Statistical analysis was performed using SigmaStat 3.3 software (Systat Software, San Jose, CA). The equality of the average distributions of adipocytes area were compared between experimental groups using Kolmogorov-Smirnov tests and exact P values computed (8). Statistical significance was designated as $P < 0.05$.

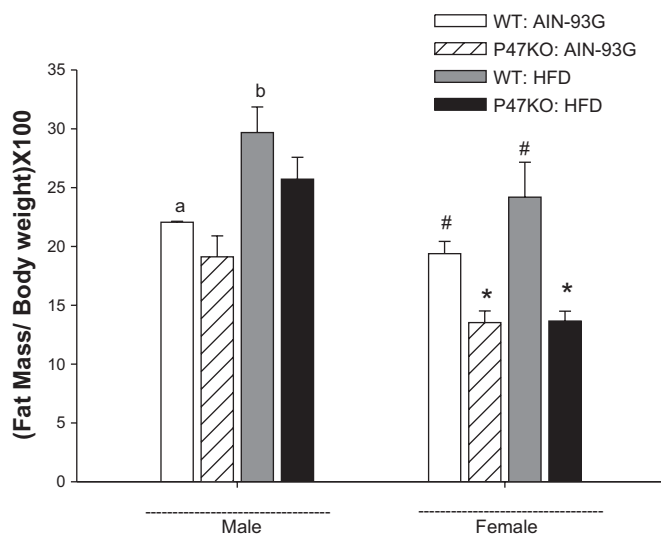


Fig. 3. NMR analysis of % fat mass in WT or P47KO mice fed AIN-93G or HFD. Data are presented as means ± SE for $n = 10$ /group. Means with different letters are statistically different for diet within genotype by 2-way ANOVA followed by Student-Newman-Keuls post hoc analysis $P < 0.05$; a < b. Means with different symbols are statistically different for genotype within each diet group $P < 0.05$; * < # by 2-way ANOVA followed by Student-Newman-Keuls post hoc analysis $P < 0.05$.

Table 3. Effect of p47^{phox} genotype and diet on mouse liver triglycerides and FA homeostasis

Group	Triglyceride, mg/g liver	SREBP-1c	FASN	CD36
<i>Male</i>				
WT: AIN-93G	124 ± 3 ^{a†}	1.8 ± 0.3 ^{b,†}	19 ± 5 ^{b,†}	4 ± 1 ^a
P47KO: AIN93G	87 ± 13*	0.9 ± 0.2*	8 ± 1*	4 ± 1 ^a
WT: HFD	197 ± 7 ^{b,†}	0.8 ± 0.1 ^a	7 ± 2 ^a	8 ± 1 ^b
P47KO: HFD	132 ± 17*	0.6 ± 0.1	5 ± 1	9 ± 1 ^b
<i>Female</i>				
WT: AIN-93G	120 ± 8 ^{a†}	1.3 ± 0.1 ^b	14 ± 2 ^{b,†}	10 ± 2 ^a
P47KO: AIN-93G	99 ± 12*	1.1 ± 0.1	8 ± 2*	8 ± 1
WT: HFD	279 ± 37 ^{b,†}	0.8 ± 0.1 ^a	8 ± 1 ^a	14 ± 1 ^{b,†}
P47KO: HFD	141 ± 15*	0.9 ± 0.1	6 ± 1	8 ± 1*

Data are means ± SE ($n = 10$ mice/group). Triglyceride content (mg/g liver); Western blot immunoprecipitation of SREBP-1c protein in liver nuclear extracts; Relative target mRNA expression/18S measured by real-time RT-PCR. Means bearing different letters differ significantly by diet within genotype, a < b; means bearing different symbols differ significantly by genotype within diet $P < 0.05$, * < †, based on 2-way ANOVA followed by Student-Neuman-Keuls post hoc analysis within each sex.

RESULTS

Absence of p47^{phox} results in reduced ROS production in SV cells isolated from fat pads. P47KO mice are a well-characterized global knockout model in which NOX2-dependent ROS production is abolished in all tissues (20, 39). SV cells from fat pads of P47KO mice had significantly lower basal production of hydrogen peroxide (resulting from the action of superoxide dismutase on NOX-generated superoxide) as measured using Amplex red than did SV cells isolated from WT mice ($P < 0.05$) (Fig. 1A). In addition, hydrogen peroxide production in response to treatment with the NOX2 activator PMA was significantly lower in P47KO compared with WT cells ($P < 0.05$) (Fig. 1B).

Absence of p47^{phox} alters growth and body composition responses of mice to high-fat feeding in a sexually dimorphic fashion. After correction for body weight, no significant effects were observed on food intake in mice of either sex during the course of the study (Table 2). In contrast, both diet and genotype effects were observed on body weight, weight gain, and body composition. WT male mice weighed slightly less than P47KO males at weaning, and this difference in absolute body weight was maintained throughout the study ($P < 0.05$

by two-way ANOVA). P47KO AIN-93G males were heavier than WT AIN93G males at death ($P < 0.05$). Both genotypes increased weight when fed HFD ($P < 0.05$) (Table 2). However, expressed as % weight gain, male WT mice gained more weight than P47KO males on either diet ($P < 0.05$), and high-fat feeding only increased weight gain significantly in the WT group ($P < 0.05$) (Table 2). Both WT and P47KO mice increased abdominal fat pad weight in HFD compared with AIN-93G fed groups (Table 2). Histomorphometric analysis of adipocyte size in abdominal fat pads revealed that WT AIN-93G males had slightly larger adipocytes than P47KO AIN-93G males (mean size 3,000–4,000 μm^2 compared with 2,000–2,500 μm^2), and size distribution was skewed in favor of adipocytes $>5,000 \mu\text{m}^2$ in male HFD groups of either genotype (Fig. 2), but this did not reach statistical significance. When fat mass was measured as a % body weight by NMR, a significant increase was observed in WT HFD males compared with WT AIN-93G males ($P < 0.05$), but this increase did not achieve statistical significance in P47KO HFD males compared with P47KO AIN-93G (Fig. 3). High-fat feeding also increased ectopic fat deposition in the liver of WT male mice. The WT HFD males had increased triglyceride content compared with the WT AIN-93G males (Table 3). In contrast, P47KO males had lower hepatic triglyceride content in both diet groups ($P < 0.05$).

Female P47KO HFD mice weighed less than WT HFD females ($P < 0.05$). P47KO females on both diets had lower % weight gain than WT females, and HFD increased weight gain in WT but not in P47KO females ($P < 0.05$) (Table 2). Moreover, P47KO females on both diets had reduced abdominal fat pad weights and lower whole body adiposity than WT females, and fat mass was not increased in the P47KO HFD group compared with P47KO female mice fed AIN-93G diets ($P < 0.05$) (Table 2, Fig. 3). Histomorphometric analysis of adipocyte size in these fat pads revealed that WT AIN-93G mice had a size distribution skewed toward larger adipocytes than P47KO AIN-93G mice ($P < 0.001$). Although adipocyte size was further increased in the female WT HFD group compared with the WT AIN-93G females and increased in male P47KO HFD mice compared with male P47KO AIN-93G mice ($P < 0.001$), there was no significant increase in adipocyte size in the female P47KO HFD group compared with the female P47KO AIN-93G group (Fig. 2). When total body fat mass was measured as a % body weight by NMR, a

Table 4. Effect of p47^{phox} genotype and diet on mouse serum parameters

Group	Glucose, mg/dl	Insulin, ng/ml	NEFA, mM	Triglycerides, mg/dl	Leptin, ng/ml	Adiponectin, $\mu\text{g/ml}$
<i>Male</i>						
WT: AIN-93G	162 ± 7 ^a	3.0 ± 0.1*	0.38 ± 0.11	169 ± 6 ^{b,†}	17.4 ± 0.6 [†]	4.7 ± 0.5
P47KO: ASIN-93G	154 ± 9	4.0 ± 0.3 ^{a,†}	0.30 ± 0.02 ^a	51 ± 5 ^{a*}	8.0 ± 0.8 ^{a*}	4.5 ± 0.4
WT: HFD	198 ± 10 ^{b,†}	3.0 ± 0.3*	0.50 ± 0.03	109 ± 11 ^{a,†}	20.2 ± 6.6	5.7 ± 0.5 [†]
P47KO: HFD	141 ± 9*	6.0 ± 0.6 ^{b,†}	0.40 ± 0.03 ^b	66 ± 5 ^{b,*}	15.7 ± 2.0 ^b	3.6 ± 0.3*
<i>Female</i>						
WT: AIN-93G	132 ± 8 ^{a*}	3.0 ± 0.1 ^b	0.33 ± 0.04	86 ± 10 [†]	16.8 ± 5.4 [†]	10.7 ± 0.5 [†]
P47: AIN-93G	160 ± 10 ^{b,†}	3.7 ± 0.2 ^b	0.40 ± 0.05	62 ± 4 ^{b,*}	2.3 ± 0.5*	6.4 ± 0.6*
WT: HFD	183 ± 6 ^{b,†}	2.1 ± 0.3 ^a	0.40 ± 0.04	83 ± 9 [†]	16.0 ± 4.7 [†]	8.1 ± 0.8 [†]
P47KO: HFD	133 ± 8 ^{a*}	3.0 ± 0.2 ^a	0.50 ± 0.04	46 ± 6 ^{a*}	3.0 ± 0.8*	6.1 ± 0.3*

Data are means ± SE ($n = 10$ mice/group). Means bearing different letter differ significantly by diet within genotype $P < 0.05$, a < b; means bearing different symbols differ by genotype within diet $P < 0.05$, * < †, based on 2-way ANOVA followed by Student-Neuman-Keuls post hoc analysis within each sex.

significant increase was observed in WT HFD females compared with WT AIN-93G females ($P < 0.05$). In contrast, % fat mass was lower in P47KO female mice in both diet groups compared with WT females ($P < 0.05$) (Fig. 3). High-fat feeding increased ectopic fat deposition in the liver of WT female mice. The WT HFD group had increased triglyceride content compared with the WT AIN-93G group (Table 3). In contrast, like the P47KO males, P47KO females had lower hepatic triglyceride content in both diet groups ($P < 0.05$).

Effect of p47^{phox} genotype and high-fat feeding on serum parameters. Data for serum glucose, NEFA, triglycerides, insulin, leptin, and adiponectin are shown in Table 4. High-fat feeding increased fasting serum glucose values ($P < 0.05$) in both WT male and female mice. In contrast, P47KO HFD males had serum glucose concentrations similar to the P47KO AIN-93G males, and P47KO HFD females had lower serum glucose than the female P47KO AIN-93G group ($P < 0.05$). Serum NEFA concentrations were slightly lower in P47KO males on either diet compared with WT males ($P < 0.05$), but no differences were found in female mice. Serum triglycerides were lower in WT HFD male mice compared with WT AIN-93G males but were much lower in P47KO mice of either sex on either diet ($P < 0.05$). Fasting serum insulin concentrations were similar in WT HFD and WT AIN-93G males but were lower in WT HFD females than WT AIN-93G females. P47KO male mice had higher serum insulin than WT males on either diet ($P < 0.05$). In contrast, P47KO females had insulin values similar to WT females on either diet. Serum leptin was lower in P47KO AIN-93G males compared with WT AIN-93G males, and serum adiponectin concentration was reduced in the P47KO HFD males compared with WT HFD males ($P < 0.05$). In contrast, both leptin and adiponectin were reduced in P47KO female mice of either sex on either diet ($P < 0.05$).

Effects of p47^{phox} genotype and high-fat feeding on energy metabolism and hepatic mitochondria. Indirect calorimetry was used to estimate substrate utilization (RER), heat or energy expenditure (EE), and cage activity levels for ~24 h in Phox mice. RER and EE were analyzed by PRCF analysis (2). Significant differences in both RER and EE were found between P47KO AIN-93G and P47KO HFD mice as shown by the EC50 values in Fig. 4, A and B. PRCF analysis showed lower RER in female P47KO AIN-93G mice compared with male P47KO:AIN-93G mice ($P < 0.001$), indicating increased fatty acid utilization but lower EE ($P < 0.001$). Both sexes responded to HFD by reducing RER and by increasing EE ($P < 0.001$). However, whereas fatty acid utilization appeared to be comparable in P47KO HFD mice of either sex, EE was increased considerably more by HFD in P47KO female mice than P47KO male mice (23% vs. 8%, $P < 0.001$). Total activity counts were not different between groups (data not shown). Using hepatic mitochondrial fractions, we found protein levels of all five mitochondrial respiratory complexes were increased in the livers of P47KO AIN-93G mice of both sexes relative to WT AIN-93G mice ($P < 0.05$). Respiratory complex expression was also higher in the female P47KO HFD group compared with the female P47KO AIN-93G group and compared with WT female mice fed either diet ($P < 0.05$). Figure 5, A and C, shows representative Western blots of the five complexes in the male and female groups respectively. Quantitation of protein expression is presented in Fig. 5, B and D. Analysis of mtTFAM mRNA expression as a marker of

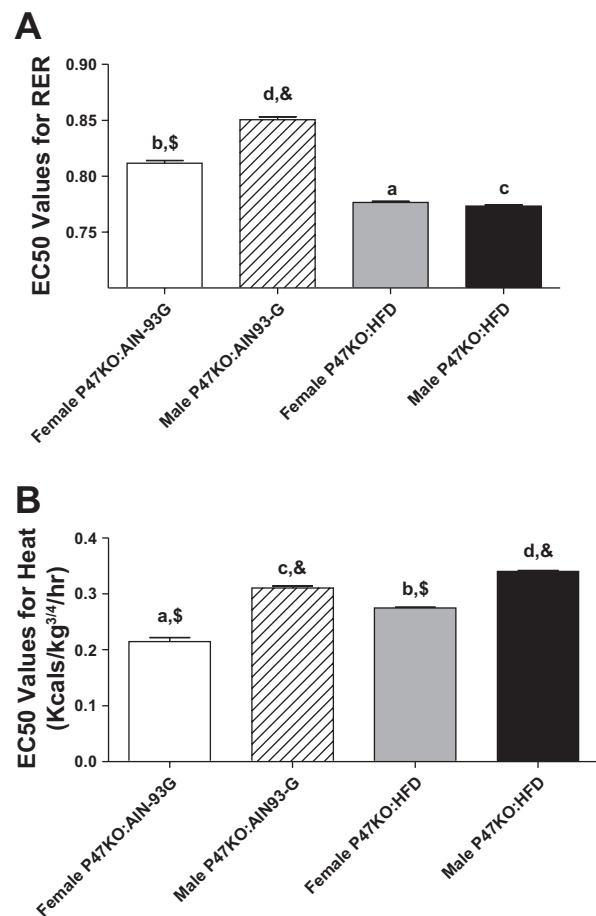


Fig. 4. Effects of feeding AIN-93G or HFD on whole body energy utilization and mitochondrial respiration in WT or P47KO mice. *A*: respiratory exchange ratio (RER) in male and female P47KO mice measured by the Complete Lab Animal Monitoring System (CLAMS) as described in MATERIALS AND METHODS. *B*: energy expenditure (Heat) in male and female P47KO mice measured by CLAMS as described in MATERIALS AND METHODS. Data represent means \pm SE for $n = 10$ /group. Means with different letters are statistically different for diet within each sex by 2-way ANOVA followed by Student-Newman-Keuls post hoc analysis $P < 0.05$; a < b; c < d. Means with different symbols are statistically different for sex within each genotype, by 2-way ANOVA followed by Student-Newman-Keuls post hoc analysis $P < 0.05$; \$ < &.

mitochondrial number demonstrated increased expression in female P47KO mice fed either diet relative to WT females ($P < 0.01$) (Fig. 6A). However, no differences in mtTFAM mRNA were observed in P47KO male mice. In addition, expression of the mRNA encoding liver mitochondrial uncoupling protein UCP-2 was increased in P47KO AIN-93G females compared with WT AIN-93G females and in both female HFD groups compared with WT AIN-93G females ($P < 0.05$) (Fig. 6B). No differences were observed in UCP-2 mRNA expression in male P47KO mice compared with male WT mice. Interestingly, expression of hepatic PGC-1 α mRNA was unchanged in female P47KO mice compared with WT female mice on either diet, and in males both HFD feeding and P47KO resulted in significantly reduced levels of PGC-1 α mRNA (Fig. 6C). Since respiration in tissues other than liver may also significantly contribute to differences in whole body energy metabolism, we also measured expression of mRNA coding for the uncoupling protein UCP-1 in brown adipose

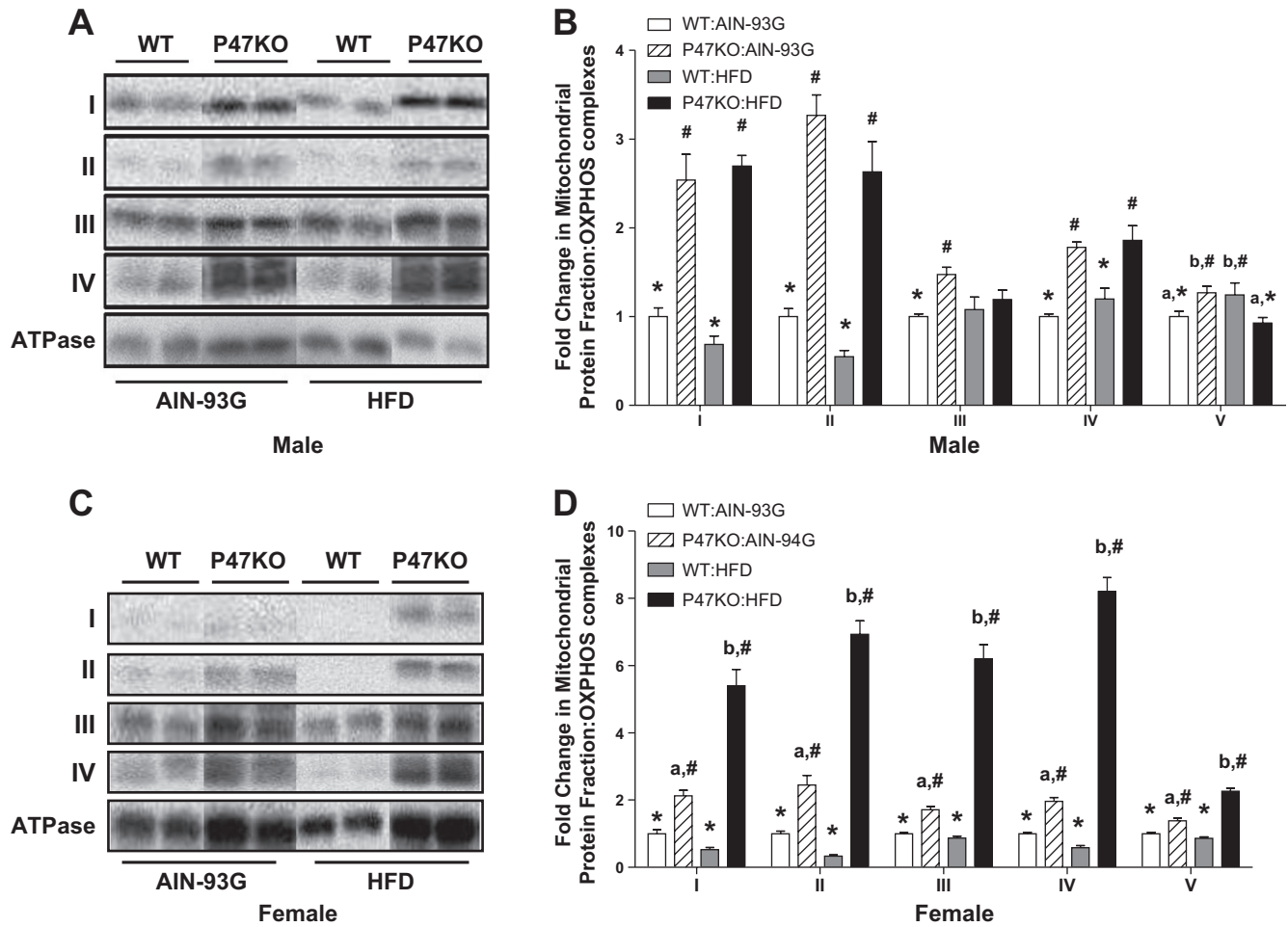


Fig. 5. A and C: representative Western immunoblots showing expression of hepatic mitochondrial respiratory complexes in male and female WT and P47KO mice fed AIN-93G or HFD diets. B and D: immunodensitometric quantification of hepatic respiratory complexes in female WT and Phox mice fed control or HFD diets. Data represent means \pm SE densitometric values for $n = 10$ /group corrected for protein loading using expression of VDAC-1 and expressed relative to WT-control = 1. Means with different letters are statistically different for diet within genotype by 2-way ANOVA followed by Student-Newman-Keuls post hoc analysis $P < 0.05$; $a < b$. Means with different symbols are statistically different for genotype within each diet group by 2-way ANOVA followed by Student-Newman-Keuls post hoc analysis $P < 0.05$; * $< \#$.

tissue of untreated WT and P47KO mice at age 6 wk. Relative expression of UCP-1 mRNA was increased in P47KO mice of both sexes: 11.7 ± 2.2 and 11.2 ± 0.4 vs. 5.1 ± 0.6 and 7.0 ± 0.3 in males and females, respectively.

Effects of p47^{phox} genotype and high-fat feeding on hepatic fatty acid synthesis and transport genes. Since P47KO mice of both sexes and on both diets had reduced hepatic triglyceride content relative to WT mice, we measured expression of

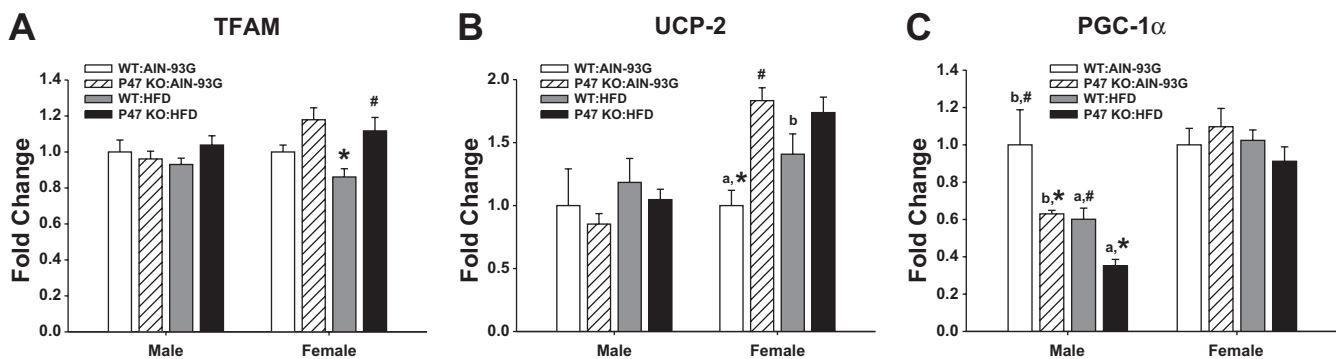


Fig. 6. Effects of feeding AIN-93G or HFD on indicators of mitochondrial number (TFAM mRNA, A), respiratory uncoupling (UCP-2 mRNA, B), and PGC-1 α mRNA (C) in the liver of male and female WT or P47KO mice. Data represent mean \pm SE values for mRNA expression of the target gene determined by real-time RT-PCR normalized to expression of 18S expressed relative to WT-control = 1 for $n = 10$ /group. Means with different letters are statistically different for diet within genotype by 2-way ANOVA followed by Student-Newman-Keuls post hoc analysis $P < 0.05$; $a < b$. Means with different symbols are statistically different for genotype within each diet group by 2-way ANOVA followed by Student-Newman-Keuls post hoc analysis $P < 0.05$; * $< \#$.

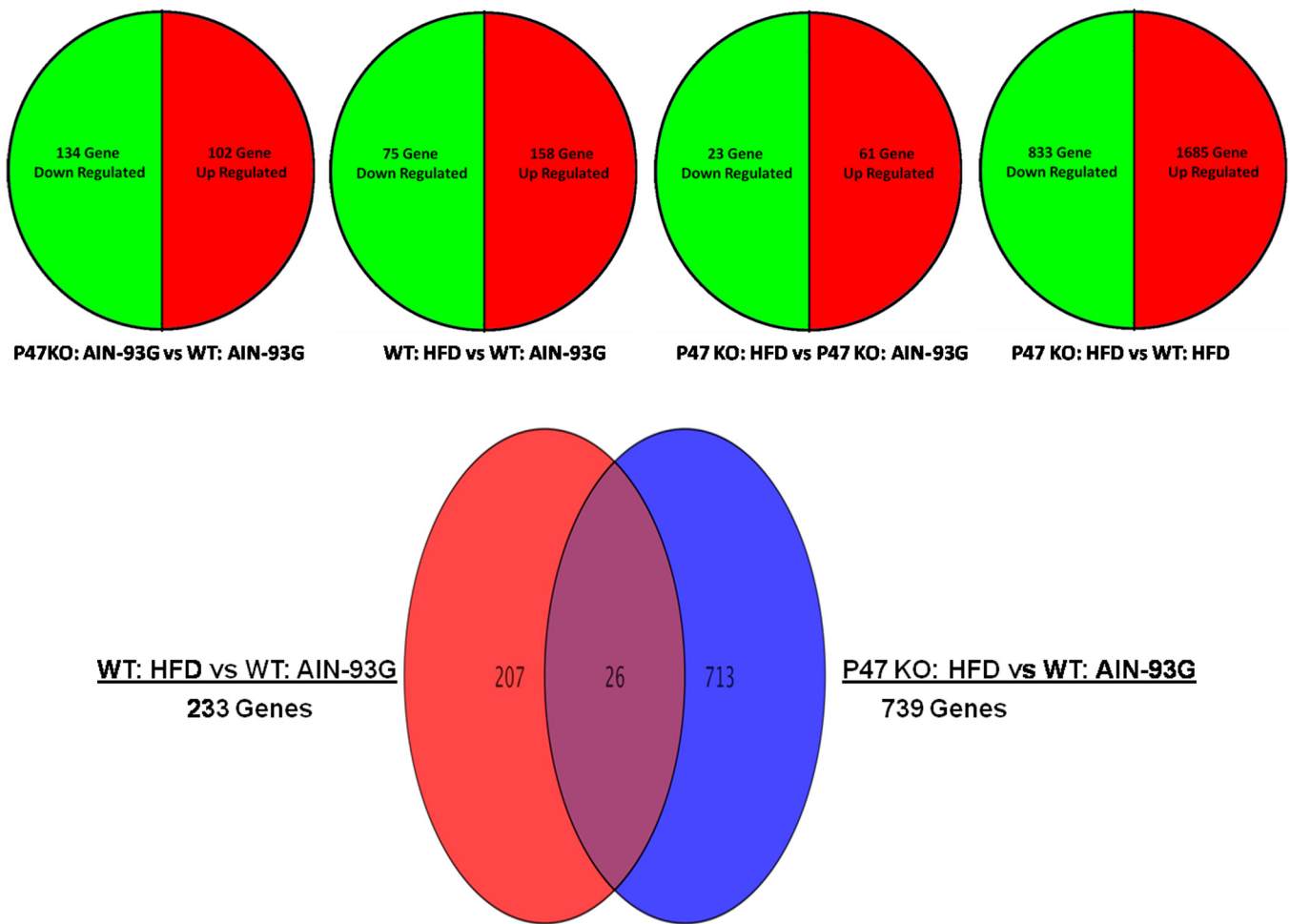


Fig. 7. Venn diagrams summarizing microarray analysis of the effects of P47KO genotype and HFD on gene expression profile in abdominal fat pads of female mice. Data in each comparison represent genes upregulated or downregulated >1.5-fold.

hepatic genes previously shown to regulate *de novo* fatty acid synthesis and fatty acid import by real-time RT-PCR (Table 3). Expression of fatty acid synthase (FASN) mRNA was reduced in P47KO AIN-93G mice of both sexes relative to WT AIN-93G mice ($P < 0.05$). High-fat feeding reduced FASN mRNA expression in WT mice ($P < 0.05$) but failed to further reduce expression in the P47KO HFD groups over the P47KO AIN-93G groups. The effect of HFD in WT mice of both sexes was accompanied by decreased expression of mRNA encoding the transcription factor sterol regulatory element binding protein (SREBP-1c) ($P < 0.05$). In contrast, there was no consistent effect of the P47^{phox} genotype on SREBP-1c mRNA expression. mRNA expression for the fatty acid transporter CD36 (14) was upregulated ($P < 0.05$) by high-fat feeding in WT mice of both sexes. In contrast, CD36 mRNA was only upregulated by high-fat feeding in male P47KO mice ($P < 0.05$).

P47^{phox} genotype alters gene expression pattern and whole genome response to high-fat feeding in female mouse adipose tissue. Since female P47KO mice had the most significantly altered body composition compared with WT mice and were completely resistant to high fat feeding-induced obesity, we examined differences in gene expression profile in retroperitoneal fat pads from WT and P47KO females fed either AIN-93G

or HFD diets using Affymetrix microarrays. The original .CEL files have been submitted to the National Center for Biotechnology Information Gene Expression Omnibus database and are accessible as series record GSE41932. The gene lists generated using a 1.5-fold cut-off are presented in Supplemental Tables S1–S4.¹ A summary of the data is presented in Fig. 7 (Venn diagrams) and Fig. 8 (hierarchical clustering and heat maps for genes involved in lipid and carbohydrate metabolism). We found 102 genes expressed more highly in the P47KO AIN93G group than in the WT AIN-93G group and 134 genes expressed at a lower level in the P47KO AIN-93G group than the WT AIN-93G group (Fig. 8). Functional annotation clustering by DAVID revealed lower expression of gene clusters linked to energy metabolism and its regulation in P47KO AIN-93G females including genes associated with insulin signaling, MAP kinase signaling, and glycolysis/gluconeogenesis (Table 5).

Analysis of the hierarchical cluster linked to carbohydrate metabolism in P47KO vs. WT AIN-93G-fed mice revealed decreased expression of enzymes in the glycolysis/gluco-kinase pathway including hexokinase (*Hk2*), enolase (*Eno1*), and

¹ The online version of this article contains supplemental material.

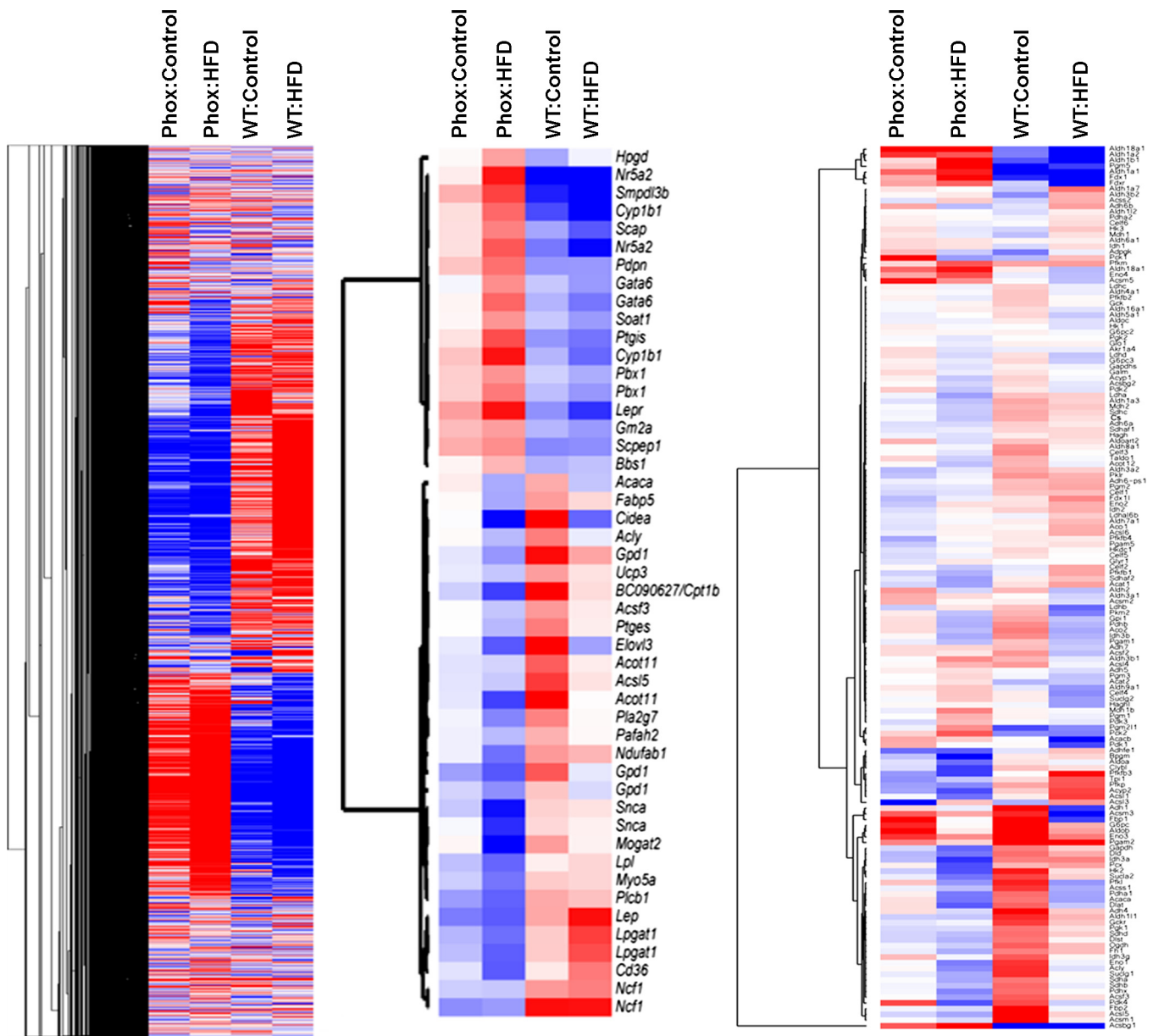


Fig. 8. Hierarchical clustering for genes exhibiting >1.5-fold change in expression in abdominal fat pads from WT and P47KO female mice fed AIN-93G or HFD. *Left*: overall clustering. *Middle*: lipid metabolism gene cluster. *Right*: carbohydrate metabolism cluster. Red, increased expression; blue, decreased expression. Complete gene lists are found in Supplemental Tables S1–S4.

phosphoglycerate kinase (*pgk1*); decreased expression of genes in the citric acid cycle including succinate dehydrogenase (*sdha*) and ATP citrate lyase (*Acly*); and decreased acyl CoA synthases (*Acss*, *Acsm*, *Acsl*). The most significantly elevated genes in this cluster in the female P47KO mice were phosphoenolpyruvate carboxykinase (*pkc1*), the rate-limiting enzyme in gluconeogenesis (42), a member of the medium chain acyl CoA synthase family (*Acsm5*), a member of the acyl CoA synthase bubblegum family (*Acsbg1*), cytochrome P450 reductase (*Fdx1*), and aldehyde dehydrogenases in families 1 and 18 involved in metabolism of retinoids and synthesis of proline (44) (Fig. 8).

Closer examination of the hierarchical cluster linked to lipid metabolism in P47KO vs. WT AIN-93G-fed mice revealed loss of expression of *Ncf1* (p47^{phox}), itself confirming the

mouse genotype, decreased fatty acid elongase (*Elov*), decreased acylCoA thiolase (*Acot*), glycerophosphate dehydrogenase (*Gpd*), and fatty acid transporter carnitine phosphatidyl transferase 1b (*Cpt1b*) (24). The response of adipose tissue to high-fat feeding in female WT mice was upregulation of 158 genes and downregulation of 75 genes, while that of female P47KO mice was upregulation of 61 genes and downregulation of 23 (Fig. 7). However, when gene expression of the female P47KO HFD and WT HFD groups was compared, 1,685 genes were expressed more highly and 833 genes were expressed at a lower level in the P47KO HFD mice ($P < 0.05$, ± 1.5 -fold). This indicates that the female adipose tissue response to high-fat feeding differed substantially by genotype and many genes were regulated in opposite directions. Indeed, when the gene expression pattern in WT HFD and P47KO HFD mice was

Table 5. DAVID analysis of adipose tissue gene expression data

KEGG Pathways	Count	%	P Value
<i>P47KO:AIN-93G vs. WT:AIN-93G (134 Downregulated Genes)</i>			
MAPK signaling pathway	8	7.33945	0.00109
Insulin signaling pathway	5	4.58716	0.01039
Endocytosis	5	4.58716	0.03644
Glycolysis/Gluconeogenesis	3	2.75229	0.06736
<i>P47KO:AIN-93G vs. WT:AIN-93G (102 Upregulated Genes)</i>			
Systemic lupus erythematosus	4	4.21053	0.01463
Cell cycle	4	4.21053	0.02596
Complement and coagulation cascades	3	3.15789	0.05454
<i>WT:HFD vs. WT:AIN-93G (75 Downregulated Genes)</i>			
Biosynthesis of unsaturated fatty acids	3	0.59055	0.00161
<i>WT:HFD vs. WT:AIN-93G (158 Upregulated Genes)</i>			
Systemic lupus erythematosus	6	0.62176	4.10E-04
<i>P47KO:HFD vs. P47KO:AIN-93G (23 Downregulated Genes)</i>			
Starch and sucrose metabolism	2	1.25786	0.03707
<i>P47KO:HFD vs. P47KO:AIN-93G (61 Upregulated Genes)</i>			
Vascular smooth muscle contraction	3	0.75949	0.0335
Biosynthesis of unsaturated fatty acids	2	0.50633	0.06397
<i>P47KO:HFD vs. WT:HFD (833 Downregulated Genes)</i>			
Long-term depression	10	0.17256	8.33E-04
Apoptosis	10	0.17256	0.0032
Chemokine signaling pathway	15	0.25884	0.00446
Pentose phosphate pathway	5	0.08628	0.01193
Phosphatidylinositol signaling system	8	0.13805	0.01544
PPAR signaling pathway	8	0.13805	0.02007
Systemic lupus erythematosus	9	0.15531	0.02734
Inositol phosphate metabolism	6	0.10354	0.03961
MAPK signaling pathway	16	0.2761	0.0442
Leukocyte transendothelial migration	9	0.15531	0.05647
Fc epsilon RI signaling pathway	7	0.12079	0.06671
Biosynthesis of unsaturated fatty acids	4	0.06903	0.06686
Gap junction	7	0.12079	0.08005
Jak-STAT signaling pathway	10	0.17256	0.08482
Long-term potentiation	6	0.10354	0.09765
<i>P47KO:HFD vs. WT:HFD (1,685 Upregulated Genes)</i>			
Arrhythmogenic right ventricular cardiomyopathy (ARVC)	15	0.14071	2.71E-05
ECM-receptor interaction	15	0.14071	8.74E-05
Cell adhesion molecules (CAMs)	19	0.17824	0.00107
Focal adhesion	21	0.197	0.00344
TGF-beta signaling pathway	12	0.11257	0.00544
Basal cell carcinoma	9	0.08443	0.00737
Dilated cardiomyopathy	12	0.11257	0.00827
Tight junction	15	0.14071	0.01078
Wnt signaling pathway	16	0.15009	0.01099
Vascular smooth muscle contraction	13	0.12195	0.0228
p53 signaling pathway	9	0.08443	0.02695
Steroid hormone biosynthesis	7	0.06567	0.02876
Hypertrophic cardiomyopathy (HCM)	10	0.09381	0.03093
Pathways in cancer	26	0.2439	0.03113
Regulation of actin cytoskeleton	19	0.17824	0.03502
Cell cycle	13	0.12195	0.03545
Pantothenate and CoA biosynthesis	4	0.03752	0.04067
Progesterone-mediated oocyte maturation	9	0.08443	0.07621
Small cell lung cancer	9	0.08443	0.07621
Axon guidance	12	0.11257	0.08163
Leukocyte transendothelial migration	11	0.10319	0.09364
<i>P47KO:HFD vs. WT:AIN-93G (287 Downregulated Genes)</i>			
Citrate cycle (TCA cycle)	7	0.33349	3.39E-06
Glycolysis/Gluconeogenesis	8	0.38113	3.84E-05

Continued

Table 5.—Continued

KEGG Pathways	Count	%	P Value
Pyruvate metabolism	5	0.23821	0.0024
PPAR signaling pathway	6	0.28585	0.00468
Insulin signaling pathway	7	0.33349	0.01215
Alzheimer's disease	8	0.38113	0.01301
Starch and sucrose metabolism	4	0.19057	0.01339
Parkinson's disease	6	0.28585	0.03739
Huntington's disease	7	0.33349	0.04159
Propanoate metabolism	3	0.14293	0.06495
Adipocytokine signaling pathway	4	0.19057	0.06622
Glycine, serine, and threonine metabolism	3	0.14293	0.07276
<i>P47KO: HFD vs. WT:AIN-93G (426 Upregulated Genes)</i>			
Vascular smooth muscle contraction	7	0.23593	0.00302
ECM-receptor interaction	6	0.20222	0.00305
Focal adhesion	8	0.26963	0.00924
Wnt signaling pathway	6	0.20222	0.03282
Chronic myeloid leukemia	4	0.13482	0.06284
Dilated cardiomyopathy	4	0.13482	0.09827

compared with the pattern in WT AIN-93G mice, the overlap was only 26 out of 233 genes in the WT HFD group and out of 729 genes in the P47KO HFD group (Figs. 7, 8). DAVID analysis indicates that genes regulating unsaturated fatty acid synthesis were downregulated by HFD in WT but upregulated by HFD in P47KO mice. In addition, genes in the pentose phosphate pathway were more highly expressed in WT HFD than P47KO HFD mice (Table 5).

Further examination of the hierarchical cluster linked to carbohydrate metabolism indicated that a number of adipose tissue genes strongly upregulated by HFD in WT mice were strongly downregulated in P47KO mice. These included *pck1*, phosphofructokinase (*Pfkfb3*, *Pfkfb*), triose phosphate isomerase (*Tpi 1*), acylphosphatase (*Acyp2*), and acyl CoA synthase (*Acs1*, *Acs3*) (Fig. 8). Likewise, in the lipid metabolism cluster, leptin (*lep*), lysophosphatidylglycerol acyltransferase (*Lpgat1*), lipoprotein lipase (*Lpl*), and the fatty acid transporter CD36 mRNAs were all highly upregulated by HFD in WT mice but were downregulated by HFD in female P47KO mice (Fig. 8). GO analysis revealed that one major pathway that differed between WT HFD and P47KO HFD groups was that involved in differentiation of mesenchymal stem cells into adipocytes or into osteoblast cells (Fig. 9). In P47KO HFD mice, expression of mRNA encoding the transcription factor PPAR γ , which positively regulates adipocyte differentiation (4), was significantly lower than in WT HFD mice. This was accompanied by reduced expression of leptin, a marker of differentiated adipocytes (Fig. 9). In contrast, mRNA encoding the transcription factor Runx2, which inhibits adipocyte differentiation and promotes stem cell differentiation into the osteoblast lineage (4), was expressed at a significantly higher level in adipose tissue from P47KO HFD mice than in adipose tissue from WT HFD mice (Fig. 9). In addition, other pro-osteoblastic genes, *Ihh* (Indian hedgehog) (10) and four-and-a half LIM 2 (*Fhl2*) (9, 16), were elevated in the P47KO HFD group compared with the WT:HFD group. *Gjal* (gap junction protein alpha 1, connexin 36), another regulator of osteoblast development (3, 22), was also elevated in the P47KO HFD group (Fig. 10). We confirmed the reduced expression of mRNAs for LPL, CD36, and PPAR γ and increased expression of Runx2 mRNA in female but not male abdominal fat pads from P47KO

AIN-93G and P47KO HFD mice compared with WT AIN-93G and WT HFD mice by real-time RT-PCR analysis (Fig. 11). In addition, reduced expression of LPL, CD36, and PPAR γ in adipose tissue from P47KO HFD females compared with WT:HFD females was confirmed at the protein level by Western immunoblot analysis of whole cell homogenates from gonadal fat pads (Fig. 12). In contrast, only expression of CD36 protein was significantly lower in gonadal fat pads from male P47KO HFD mice compared with male WT HFD mice (Fig. 12).

Ex vivo adipogenesis is suppressed significantly more by 17 β -estradiol treatment in cells derived from female P47KO mice than in cells derived from female WT mice. SV cells (preadipocytes) isolated from the retroperitoneal abdominal fat pads of untreated WT and P47KO mice at age 6 wk were differentiated into adipocytes *ex vivo* in the presence or absence of 1 nM 17 β -estradiol (E2). Differentiated adipocytes identified by oil red O staining of accumulated triglyceride were counted and representative staining in cells from WT and P47KO female mice are shown in Fig. 9, A–F. Quantification of triplicate cultures is shown in Fig. 9G. In the absence of E2, adipogenesis occurred at similar rates in cells from both WT and P47KO mice. Moreover, in SV cells derived from either sex and from both genotypes, E2 treatment suppressed adipogenesis ($P < 0.05$). E2 suppressed adipogenesis to the same extent in cells from WT and P47KO males. However, in cells derived from female mice, E2 suppressed adipogenesis significantly more in cells from P47KO mice than in cells derived from WT mice ($P < 0.05$). Cells from P47KO mice expressed higher levels of mRNA encoding the antiadipogenic factor preadipocyte factor-1 (Pref-1) than cells from WT mice of either sex ($P < 0.05$). In addition, E2 treatment increased Pref-1 mRNA expression more in cells from P47KO mice than in cells from WT mice ($P < 0.05$) (Fig. 9H).

DISCUSSION

In this study, we show that loss of p47^{phox} results in a sexually dimorphic alteration in metabolic homeostasis. Since p47^{phox} is an essential cofactor required for NOX2, these effects are assumed to be related to reductions in NOX2-

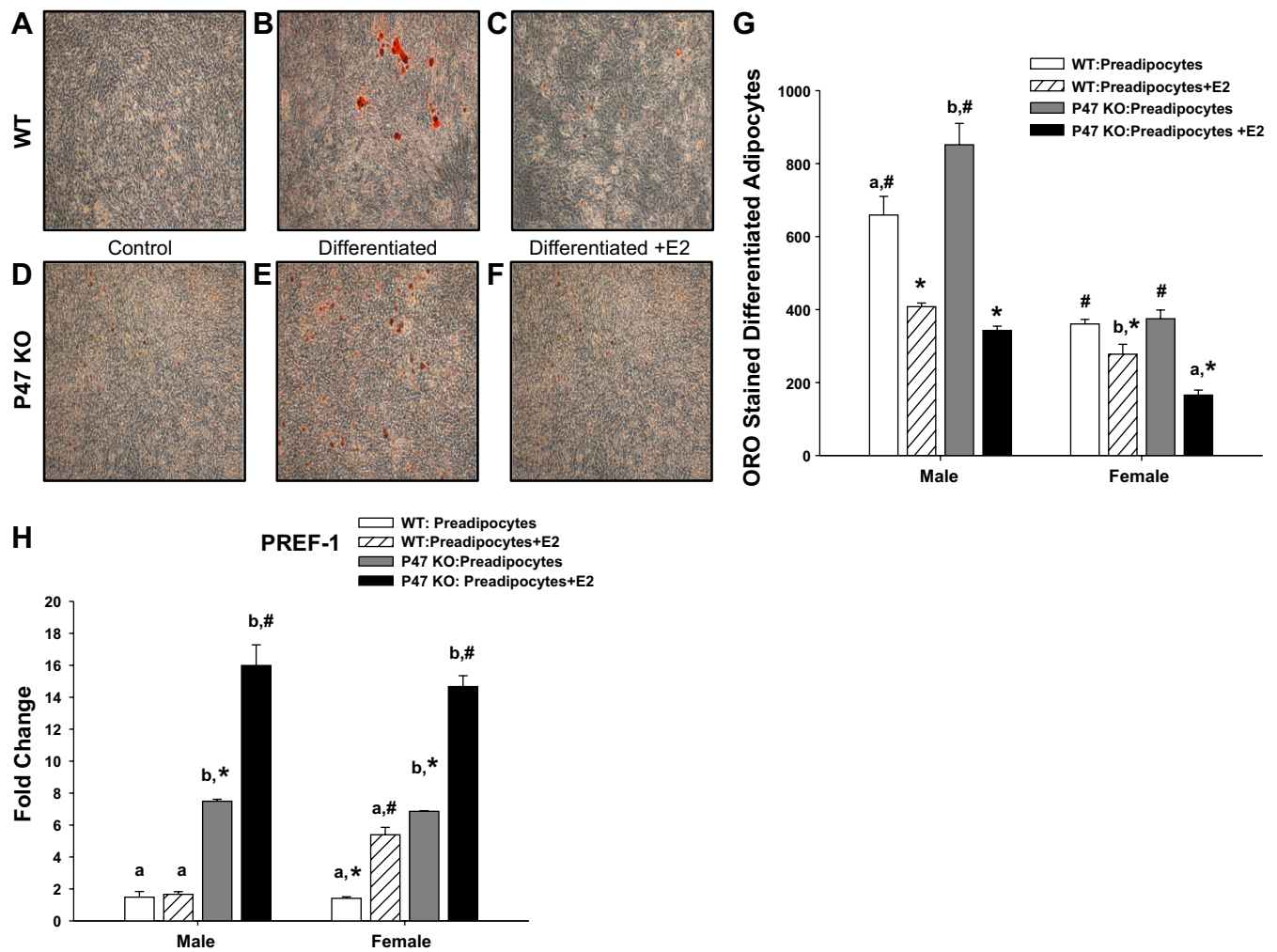


Fig. 9. Ex vivo adipogenesis of SV cells isolated from fat pads of untreated male and female WT and P47KO mice age 6 wk. *A–F*: representative oil red O (ORO)-stained cultures following differentiation in the presence or absence of 1 nM 17 β -estradiol (E2) as described in MATERIALS AND METHODS. *G*: quantification of ORO-stained adipocytes after differentiation. *H*: relative expression of Pref-1 mRNA in SV cell cultures normalized to expression of 18S. Means with different letters are statistically different for diet within genotype by 2-way ANOVA followed by Student-Newman-Keuls post hoc analysis $P < 0.05$; a < b. Means with different symbols are statistically different for genotype within each diet group by 2-way ANOVA followed by Student-Newman-Keuls post hoc analysis $P < 0.05$; * < #.

associated ROS production. Both male and female P47KO mice were resistant to development of HFD-induced hyperglycemia and hepatic steatosis. However, female P47KO mice had significantly lower adipocyte size and decreased latent adipose tissue accumulation and were resistant to diet-induced obesity. These sexually dimorphic effects involving presence or absence of NOX2 signaling may have important implications for interventions in obesity.

P47KO mice fed AIN-93G diets were slightly heavier than WT mice at weaning, but male P47KO mice gained slightly less weight during the 13 wk feeding period without a difference in total body % fat mass. In contrast, P47KO female mice gained much less weight than WT females and were significantly leaner. Challenge with HFD diets resulted in obesity in WT mice of both sexes, and whereas there was a marginal reduction in adiposity in HFD P47KO males compared with HFD WT males, P47KO females were completely resistant to both the obesogenic effects of HFD. This P47KO body fat mass phenotype was independent of changes in food intake,

despite dramatic decreases in serum leptin concentrations that might be expected to stimulate appetite. It has been suggested that ROS production in the hypothalamus is critical for appetite regulation (12), and a potential role for NOX2 in this process remains a subject for future investigations.

Rather than the result of changes in caloric intake, our data are consistent with increased uncoupled respiration, decreases in energy efficiency, reduced capacity of adipose tissue to take up circulating fatty acids, and suppressed adipose tissue differentiation as potential mechanisms underlying the dramatic body composition differences between female P47KO and WT mice. Comparison of energy metabolism in male and female P47KO mice by indirect calorimetry revealed an underutilization of carbohydrates by P47KO females when fed high-carbohydrate diets, which could contribute to reduced energy efficiency. Consistent with whole body energy metabolism data, gene arrays in adipose demonstrated lower expression glycolysis and citric acid cycle genes and increased expression of *Pck1* consistent with elevated gluconeogenesis by P47KO

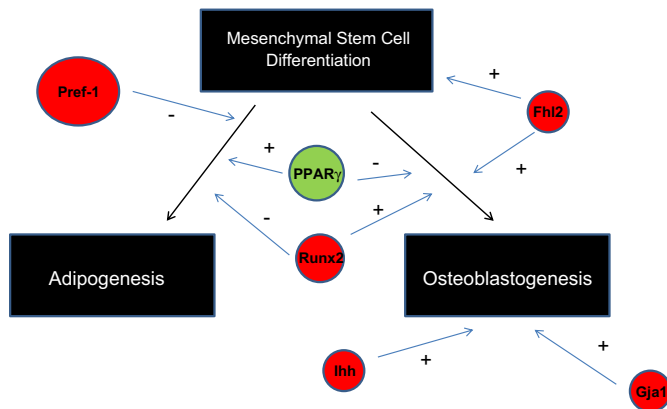


Fig. 10. The effects of P47KO genotype on expression of genes regulating differentiation of mesenchymal stem cells to adipocytes or osteoblasts in abdominal fat pads of female mice fed HFD. Green, downregulated >1.5-fold in P47KO HFD vs. WT HFD group. Red, upregulated >1.5-fold in P47KO HFD vs. WT HFD group.

females. RER data suggest that, after HFD feeding, both male and female P47KO mice demonstrated a similar degree of metabolic flexibility in switching to utilization of fatty acids. However, female P47KO HFD mice had a greater increase in EE relative to WT HFD females compared with the effect of genotype in HFD males, consistent with the increased uncoupling of hepatic respiration indicated by increased expression of *UCP-2* mRNA. Both sexes of P47KO mice exhibited increased expression of *UCP-1* mRNA in brown adipose tissue, suggesting tissue-specific effects of the P47KO genotype on respiratory uncoupling. Moreover, analysis of expression of respiratory complexes suggests that female P47KO mice had a much greater increase in mitochondrial respiration in response to HFD than that seen in P47KO males or in WT female mice, and increased expression of mTfAM mRNA suggests an additional significant increase in mitochondrial number. However, possible changes in mitogenesis appear to be independent of increases in expression of PGC-1 α . A complete understanding of how NOX2-dependent ROS signaling regulates pathways of carbohydrate and fat metabolism, mitochondrial respiration, and uncoupling in liver, skeletal muscle, and fat will require direct measures of respiratory rates in vivo and in vitro and additional analysis of mRNA and protein expression. This remains the important subject of additional studies.

Increases in uncoupled respiration could significantly contribute to the improved metabolic and biochemical outcomes after HFD including protection against development of hyperglycemia, reductions in serum triglycerides, and protection against development of hepatic steatosis. Previous studies have also demonstrated protection against HFD-induced systemic insulin resistance in male P47KO mice (43). However, in the case of steatosis, other factors also appear to play a role. Both male and female P47KO HFD mice were equally resistant to HFD-induced accumulation of hepatic triglycerides. Moreover, both sexes of P47KO mice had significantly reduced hepatic fatty acid synthesis as indicated by reduced expression of *FASN* mRNA. Molecular mechanisms underlying this effect require further investigation but appear not to involve differences in signaling through SREBP-1c. In female P47KO mice, in addition, there appears to be an impairment of HFD effects on fatty acid transport since HFD-induction of *CD36* mRNA was also impaired. Our data are consistent with a recent study demonstrating protection of P47KO mice against the development of hepatic steatosis produced by alcohol treatment (20). Interestingly, in that study the protection afforded by p47^{phox} deficiency was associated with p47^{phox} expression in liver parenchymal cells rather than in nonparenchymal cells such as Kupffer cells or liver macrophages. It remains to be seen if the same is true in regards to HFD-driven steatosis. However, as in the current study, protection against development of alcoholic steatosis was linked to effects on fatty acid synthesis and *FASN* expression (20).

Both control and HFD-fed P47KO female mice had reduced % total body fat mass, fat pad weight, and adipose cell size compared with WT females. Some of the sexually dimorphic effects of p47^{phox} absence on adipocyte hypertrophy appeared to be associated with reduced uptake of fatty acids. Both LPL, which is involved in hydrolysis of serum triglycerides to fatty acids for adipocyte uptake (45), and *CD36*, which transports free fatty acids into adipocytes (35), were suppressed at the mRNA and protein level. Both enzymes are downstream targets of the transcription factor PPAR γ (35, 46). Suppression of PPAR γ mRNA (and PPAR γ protein) and of leptin expression in female P47KO mice indicates reduced adipocyte differentiation accompanied by evidence of enhanced MSC differentiation in favor of the osteoblast lineage (increased *Runx2*, *Ihh*, and *Flm2* mRNAs).

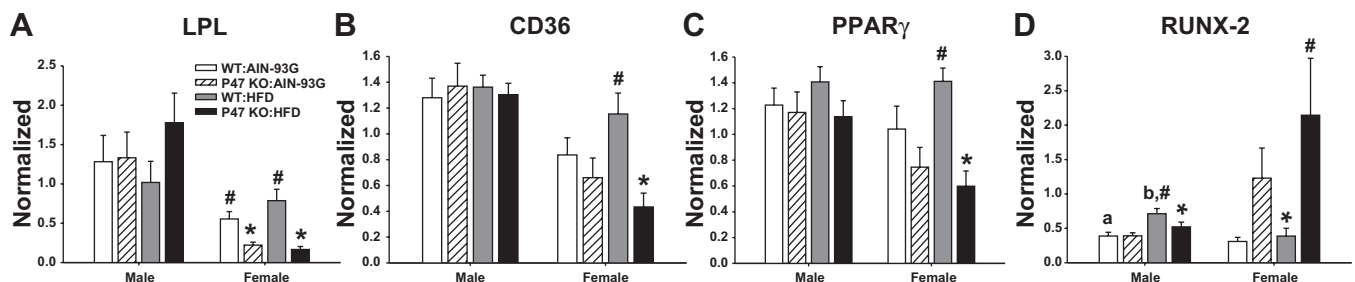


Fig. 11. Effects of feeding AIN-93G or HFD on genes regulating adipose tissue fatty acid uptake. A: lipoprotein lipase (LPL) mRNA. B: *CD36* mRNA and mesenchymal stem cell differentiation into adipocytes. C: PPAR γ mRNA or into osteoblasts. D: *Runx-2* mRNA in abdominal fat pads of male and female WT or female P47KO mice. Data represent mean \pm SE values for mRNA expression of the target gene determined by real-time RT-PCR normalized to expression of 18S for $n = 10$ /group. Means with different letters are statistically different for diet within genotype by 2-way ANOVA followed by Student-Newman-Keuls post hoc analysis $P < 0.05$; $a < b$. Means with different symbols are statistically different for genotype within each diet group by 2-way ANOVA followed by Student-Newman-Keuls post hoc analysis $P < 0.05$; * < #.

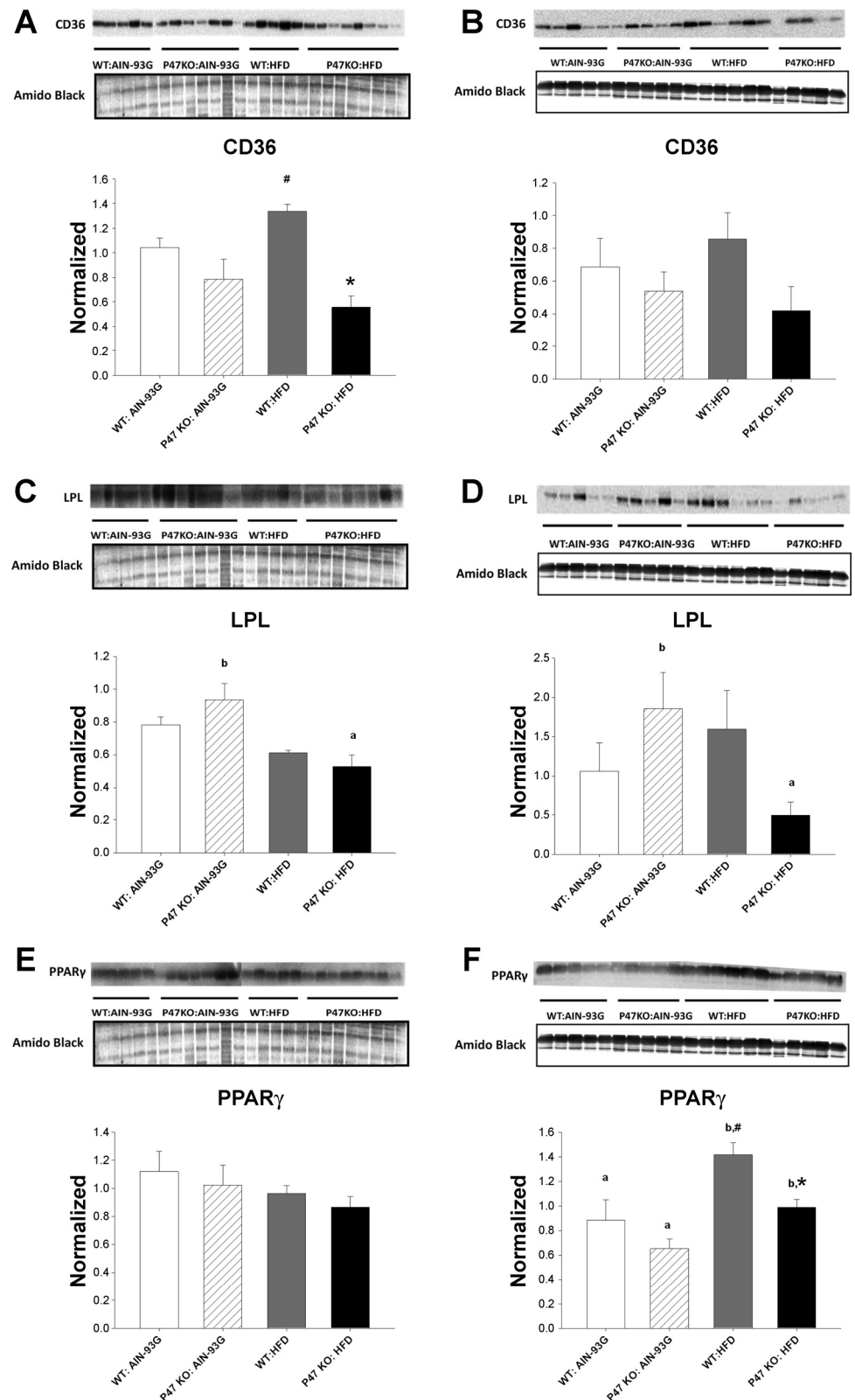


Fig. 12. Effects of feeding AIN-93G or HFD on expression of proteins regulating adipose tissue fatty acid uptake. *A* and *B*: CD36 mRNA. *C* and *D*: LPL mRNA and mesenchymal stem cell differentiation into adipocytes. *E* and *F*: PPAR γ mRNA in gonadal fat pads from male (*A*, *C*, *E*) and female (*B*, *D*, *F*) WT or female P47KO mice. Western blots show samples from a different animal in each lane. Data represent mean \pm SE values for protein expression in Western immunoblots of whole tissue homogenates ($n = 5/\text{group}$) normalized to protein loading as determined by Amido black staining of membranes. Means with different letters are statistically different for diet within genotype by 2-way ANOVA followed by Student-Newman-Keuls post hoc analysis $P < 0.05$; $a < b$. Means with different symbols are statistically different for genotype within each diet group by 2-way ANOVA followed by Student-Newman-Keuls post hoc analysis $P < 0.05$; $* < \#$.

Our ex vivo adipogenesis experiments with adipose tissue-derived SV cells support the hypothesis that differentiation of preadipocytes is regulated by NOX2-dependent ROS signaling and negative cross talk between NOX2 signaling and E2

signaling pathways. We have previously reported negative cross talk between NOX-mediated ROS signaling and estrogen receptor signaling in osteoblasts (5). In SV cells from female mice, E2 suppression of adipogenesis was significantly en-

hanced by in the P47KO mice consistent with the obesity resistant phenotype of these mice in vivo. Interestingly, inhibition of adipogenesis was correlated with increased E2 induction of the antiadipogenic factor Pref-1, which is upstream of PPAR γ in adipocyte differentiation (39a, 41) (Fig. 9). In the absence of E2, there was no difference in adipogenesis of SV cells derived from WT and P47KO mice. This is consistent with the lack of protection against HFD-driven obesity in male mice where E2 levels are low. However, the molecular mechanisms underlying the effects of E2 and ROS on adipogenesis are complex, and further work is required for a complete understanding of these pathways.

ROS signaling has previously been linked to adipocyte differentiation from mesenchymal stem cells (MSCs) in vitro. Kanda et al. (13) reported ROS formation during insulin-induced differentiation of 10T1/2 cells into adipocytes and blockage of adipocyte differentiation of both 10T1/2 cells and primary rat bone marrow-derived MSCs by the antioxidant N-acetylcysteine. Moreover, these authors and Schroeder et al. (36) ascribed the ROS production in MSCs and preadipocytes to NOX activity. However, the NOX they identified as the driver of adipogenesis was NOX4 not NOX2. The presence of multiple NOX enzymes (NOX1, NOX2, and NOX4) has previously been described in preadipocytes and mature adipocytes (13, 23, 36). However, the interaction between different NOX regulated ROS pathways in the same cell appears to be complex. Some authors have suggested that constitutively active NOX4 acts as an oxygen sensor and that NOX4-mediated ROS signaling results in downstream activation of NOX1 and NOX2 and amplification of the ROS signal through recruitment of the cytosolic phox activator proteins and the Rac1 GTPase (29). Moreover, there is evidence in some cell types, such as preosteoclasts and chondrocytes, that multiple NOX enzymes can compensate for each other in the same pathway (15, 33). However, in other cells, NOX4 and NOX2 appear to regulate separate pathways via different sets of MAP kinases (1). Recent studies of male NOX4-deficient mice in vivo have demonstrated a phenotype contradictory to in vitro studies of insulin-dependent adipogenesis. These mice are highly susceptible to high fat-driven obesity and steatosis and have reduced adipocyte differentiation and increased energy efficiency (21). This phenotype is the opposite of that displayed by female p47^{phox} knockout mice in the current study. These data suggest that NOX4 and NOX2 ROS signals may have opposite actions on the same pathways regulating energy homeostasis and adipocyte differentiation.

In summary, this study examined the consequence of loss of NOX2-dependent ROS production on body composition and whole body metabolic and energy homeostasis indirectly by determining the phenotype of mice lacking p47^{phox}, an essential cytosolic NOX2 activator protein. The results demonstrate that loss of p47^{phox} triggers a complex metabolic and sexually dimorphic phenotype with female predominant reduction of adipose tissue hypertrophy and resistance to HFD-induced obesity. These data are consistent with a role for ROS signaling in maintenance of whole body energy homeostasis but suggest that the interaction of NOX2 and NOX4-dependent ROS pathways in this phenomenon is complex and appears antagonistic. Greater understanding of the ROS signaling pathways regulating adipogenesis and adipose tissue hypertrophy may also

result in identification of novel molecular targets for obesity prevention and anti-obesity therapies.

ACKNOWLEDGMENTS

We thank the following people for technical assistance Trae Pittman, Courtney Mosley, Forrest Lindsey, Heather Clarke, Bobby Fay, and Rene Till.

GRANTS

This research was supported in part by ACNC-USDA-ARS-CRIS 6251-51000-005-004S (website: <http://ars.usda.gov>). "The funders had no role in study design, data collection, decision to publish or preparation of the manuscript".

DISCLOSURES

No conflicts of interest, financial or otherwise, are declared by the author(s).

AUTHOR CONTRIBUTIONS

Author contributions: M.J.J.R. and T.M.B. conception and design of research; M.J.J.R., N.S., J.V., S.J.B., M.F., K.E.M., M.A.C., H.G.-A., and T.M.B. analyzed data; M.J.J.R., S.J.B., K.E.M., H.G.-A., and T.M.B. interpreted results of experiments; M.J.J.R., N.S., J.V., S.J.B., and H.G.-A. prepared figures; M.J.J.R. drafted manuscript; M.J.J.R., N.S., J.V., S.J.B., M.F., M.A.C., H.G.-A., and T.M.B. edited and revised manuscript; M.J.J.R., N.S., J.V., S.J.B., M.F., K.E.M., M.A.C., H.G.-A., and T.M.B. approved final version of manuscript; N.S., J.V., M.F., and K.E.M. performed experiments.

REFERENCES

1. Anikumar N, Weber R, Zhang M, Brewer A, Shah AM. Nox4 and Nox2 NADPH oxidases mediate distinct cellular redox signaling responses to agonist stimulation. *Arterioscler Thromb Vasc Biol* 28: 1347–1354, 2008.
2. Borengasser SJ, Lau F, Kang P, Blackburn ML, Ronis MJ, Badger TM, Shankar K. Exposure to maternal obesity during gestation impairs fatty acid oxidation and mitochondrial SIRT3 expression in the offspring at weaning. *PLoS One* 6: e24068, 2011.
3. Chaible LM, Sanches DS, Cogliati B, Menecier G, Dagli ML. Delayed osteoblastic differentiation and bone development in Cx43 knockout mice. *Toxicol Pathol* 39: 1046–1055, 2011.
4. Chen JR, Lazarenko OP, Blackburn ML, Badger TM, Ronis MJ. A role for ethanol-induced oxidative stress in controlling lineage commitment of mesenchymal stromal cells through inhibition of Wnt/beta catenin signaling. *J Bone Miner Res* 25: 1117–1127, 2010.
5. Chen JR, Lazarenko OP, Haley RL, Blackburn ML, Badger TM, Ronis MJ. Ethanol impairs estrogen receptor signaling and activates senescence pathways in osteoblasts. Protection by estradiol. *J Bone Miner Res* 24: 221–230, 2009.
6. Cross AR, Segal AW. The NADPH oxidase of professional phagocytes - prototype of the NOX electron transport chain systems. *Biochim Biophys Acta* 1657: 1–22, 2004.
7. Furukawa S, Fujita T, Shimabukuro M, Iwaki M, Yamada Y, Nakajima Y, Nakayama O, Makishima M, Matsuda M, Shimomura I. Increased oxidative stress in obesity and its impact on metabolic syndrome. *J Clin Invest* 114: 1752–1761, 2004.
8. Gibbons JD, Chakraborti S. *Nonparametric Statistical Inference* (5th Ed.). Boca Raton, FL: Chipman & Hall/CRC, 2011.
9. Govoni KE, Baylink DJ, Chen J, Mohan S. Disruption of four and a half LIM 2 decreases bone mineral content and bone mineral density in femur and tibia bones of female mice. *Calcif Tissue Int* 79: 112–117, 2006.
10. Gunther T, Schinke T. Mouse genetics have uncovered new paradigms in bone biology. *Trends Endocrinol Metab* 11: 189–193, 2000.
11. Haesegawa T, Kikuyama M, Sakurai K, Kambayashi Y, Adachi M, Saniabadi AR, Kuwano H, Nakano M. Mechanism of superoxide anion production by hepatic sinusoidal epithelial cells and Kupffer cells during short term ethanol perfusion in the liver. *Liver* 22: 321–329, 2002.
12. Horvath TL, Andrews ZB, Diano S. Fuel utilization by hypothalamic neurons: role for ROS. *Trends Endocrinol Metab* 20: 78–87, 2009.
13. Kanda Y, Hinata T, Kang SW, Watanabe Y. Reactive oxygen species mediate adipocyte differentiation in mesenchymal stem cells. *Life Sci* 89: 250–258, 2011.

14. Kennedy DJ, Kashyap SR. Pathogenic role of scavenger receptor CD36 in the metabolic syndrome and diabetes. *Metab Syndr Relat Disord* 9: 239–245, 2011.
15. Kim KS, Choi HW, Yoon HE, Kim IY. Reactive oxygen species generated by NADPH oxidase 2 and 4 are required for chondrogenic differentiation. *J Biol Chem* 285: 40294–40302, 2010.
16. Lai CF, Bai S, Uthgenannt BA, Halstead LR, McLoughlin P, Schafer BW, Chu PH, Chen J, Otey CA, Cao X, Cheng SL. Four and half lim protein 2 (FHL2) stimulates osteoblast differentiation. *J Bone Miner Res* 21: 17–28, 2006.
17. Lee OH, Seo MJ, Choi HS, Lee BY. Pycnogenol inhibits lipid accumulation in 3T3–L1 adipocytes with the modulation of reactive oxygen species (ROS) production associated with antioxidant enzyme responses. *Phytother Res* 26: 403–411, 2012.
18. Lee YH, Nair S, Rousseau E, Allison DB, Page GP, Tataranni PA, Bogardus C, Permana PA. Microarray profiling of isolated abdominal subcutaneous adipocytes from obese vs. non-obese Pima Indians: increased expression of inflammation-related genes. *Diabetologia* 48: 1776–1783, 2005.
19. Leto TL, Morand S, Hurt D, Ueyama T. Targeting and regulation of reactive oxygen species generation by Nox family NADPH oxidases. *Antioxid Redox Signal* 11: 2607–2619, 2009.
20. Levin I, Petrusek J, Szabo G. The presence of p47^{phox} in liver parenchymal cells is a key mediator in the pathogenesis of alcoholic liver steatosis. *Alc Clin Exp Res* 36: 1397–1406, 2012.
21. Li Y, Mouche S, Sajic T, Veyrat-Durebex C, Supale R, Pierroz D, Ferrari S, Negro F, Hasler U, Feraille E, Moll S, Meda P, Deffert C, Montet X, Krause KH, Szanto I. Deficiency in the NADPH oxidase 4 predisposes towards diet-induced obesity. *Int J Obesity* 36: 1503–1513, 2012.
22. Li Z, Zhou Z, Saunders MM, Donahue HJ. Modulation of connexin43 alters expression of osteoblastic differentiation markers. *Am J Physiol Cell Physiol* 290: C1248–C1255, 2006.
23. Lin L, Pang W, Chen K, Wang F, Gengler J, Sun Y, Tong Q. Adipocyte expression of PU.1 transcription factor causes insulin resistance through upregulation of inflammatory cytokine gene expression and ROS production. *Am J Physiol Endocrinol Metab* 302: E1550–E1559, 2012.
24. Longo N, Amat di San Filippo C, Pasquali M. Disorders of carnitine transport and the carnitine cycle. *Am J Med Genet C Semin Med Genet* 142C: 77–85, 2006.
25. Matsuzawa-Nagata N, Takamura T, Ando H, Nakamura S, Kurita S, Misu H, Ota T, Yokoyama M, Honda M, Miyamoto K, Kaneko S. Increased oxidative stress precedes the onset of high fat diet-induced insulin resistance and obesity. *Metabolism* 57: 1071–1077, 2008.
26. Park HS, Jin DK, Shin SM, Jang MK, Longo N, Park JW, Bae DS, Bae YS. Impaired generation of reactive oxygen species in leprechaunism through downregulation of Nox4. *Diabetes* 54: 3175–3181, 2005.
27. Peshvariya HM, Dusting GJ, Selemidis S. Analysis of dihydroethidium fluorescence for the detection of intracellular and extracellular superoxide produced by NADPH oxidase. *Free Radic Res* 41: 699–712, 2007.
28. Petry A, Djordjevic T, Weitnauer M, Kietzmann T, Hess J, Gorrlich A. NOX2 and NOX4 mediate proliferative response in endothelial cells. *Antioxid Redox Signal* 8: 1473–1484, 2006.
29. Piccoli C, D'Aprile A, Scrima R, Ripoli M, Boffoli D, Tabilio A, Caitanio N. Role of reactive oxygen species as signal molecules in the pre-commitment phase of adult stem cells. *Ital J Biochem* 56: 295–301, 2007.
30. Ronis MJJ, Baumgardner JN, Marecki J, Hennings L, Wu X, Shankar K, Cleves MA, Gomez-Acevedo H, Badger TM. Dietary fat source alters hepatic gene expression profile and determines the type of liver pathology in rats overfed via total enteral nutrition. *Physiol Genomics* 44: 1073–1089, 2012.
31. Ronis MJJ, Chen Y, Shankar K, Gomez-Acevedo H, Badeaux J, Blackburn ML, Badger TM. Formula feeding and protein source alter hepatic gene expression, iron and cholesterol homeostasis in neonatal piglets. *Physiol Genomics* 43: 1281–1293, 2011.
32. Ronis MJJ, Rowlands JC, Hakkak R, Badger TM. Altered inducibility of hepatic CYP1A enzymes by 3-methylcholanthrene and isosafrole in male rats fed diets containing casein, soy protein isolate or whey. *J Nutr* 131: 1180–1188, 2001.
33. Sasaki H, Yamamoto H, Toiminaga K, Masuda K, Kawai T, Teshima-Kondo S, Matsuno K, Yabe-Nishimura C, Rokutan K. Receptor activator of nuclear factor-kappaB ligand-induced mouse osteoclast differentiation is associated with switching between NADPH-oxidase homologues. *Free Radic Biol Med* 47: 189–199, 2009.
35. Schoonjans K, Staels B, Auwerx J. The peroxisome proliferator activated receptors (PPARs) and their effects on lipid metabolism and adipocytes differentiation. *Biochim Biophys Acta* 1302: 93–109, 1996.
36. Schroeder K, Wandzioch K, Helmcke I, Brandes RP. Nox4 acts as a switch between differentiation and proliferation in preadipocytes. *Arterioscler Thromb Vasc Biol* 29: 239–245, 2009.
37. Shankar K, Harrell A, Liu X, Gilchrist J, Ronis MJJ, Badger TM. Maternal obesity at conception programs obesity in the offspring. *Am J Physiol Regul Integr Comp Physiol* 294: R528–R538, 2008.
38. Shankar K, Harrell A, Kang P, Zhong Y, Marecki JC, Ronis MJJ, Badger TM. Maternal overweight programs insulin and adiponectin signaling in the offspring. *Endocrinology* 151: 2577–2589, 2010.
39. Silver AE, Beske SD, Christu DD, Donato AJ, Moreau KL, Eskurza I, Gates PE, Seals DR. Overweight and obese humans demonstrate increased vascular endothelial NADPH oxidase - p47^{phox} expression and evidence of endothelial oxidative stress. *Circulation* 115: 627–637, 2007.
- 39a. Smas CM, Chen L, Zhao L, Latasa MJ, Sul HS. Transcriptional repression of pref-1 by glucocorticoids promotes 3T3–L1 adipocyte differentiation. *J Biol Chem* 274: 12632–12641, 1999.
40. Wagoner B, Hausman DB, Harris RB. Direct and indirect effects of leptin on preadipocyte proliferation and differentiation. *Am J Physiol Regul Integr Comp Physiol* 290: R1557–R1564, 2006.
41. Wang Y, Kim KA, Kim-H, Sul HS. Pref-1, a preadipocyte secreted factor that inhibits adipogenesis. *J Nutr* 136: 2953–2956, 2006.
42. Xiong Y, Lei QY, Zhao S, Guan KL. Regulation of glycolysis and gluconeogenesis by acetylation of PKM and PEPCK. *Cold Spring Harb Symp Quant Biol* 76: 285–289, 2011.
43. Xu X, Yavar Z, Verdin M, Ying Z, Mihai G, Kampfath T, Wang A, Zhong M, Lippmann M, Chen LC, Rajagopalan S, Sun Q. Effect of early particulate air pollution exposure on obesity in mice: role of P47^{phox}. *Arterioscler Thromb Vasc Biol* 30: 2518–2527, 2010.
44. Yasmeen R, Reichert B, Deullis J, Yang F, Lynch A, Meyers J, Sharlach M, Shin S, Volz KS, Green KB, Lee K, Alder H, Duyster G, Zechner R, Rajagopalan S, Ziouzenkova O. Autocrine function of aldehyde dehydrogenase 1 as a determinant of diet and sex-specific differences in visceral adiposity. *Diabetes* 62: 124–36, 2013.
45. Zechner R, Strauss J, Frank S, Wagner E, Hofmann W, Kratky D, Hiden M, Levak-Frank S. The role of lipoprotein lipase in adipose tissue development and metabolism. *Int J Obes Relat Metab Disord* 24: S53–S56, 2000.
46. Zhou J, Febbraio M, Wada T, Zhai Y, Kuruba R, He J, Lee JH, Khadem S, Ren S, Silverstein RL, Xie W. Hepatic fatty acid transporter CD36 is a common target of LXR, PXR and PPAR γ in promoting steatosis. *Gastroenterology* 134: 556–567, 2008.